aerospace

MDPI

Article

Robust Multi-Phase Vertical Recovery Guidance for Reusable Launch Vehicles Integrated with Full-Flight Fuel Consumption Prediction

Jiahao Gan [1,2,3,*], Yuanpeng Fang [2,3], Tie Su [2] and Jin Zhang [2]

[1] School of Aeronautical Science and Engineering, Beihang University, Beijing 100083, China
[2] AVIC Chengdu Aircraft Design and Research Institute, Chengdu 610091, China; fypeng7512@163.com (Y.F.); unliver1@163.com (T.S.); gbjy1302@163.com (J.Z.)
[3] Aviation Key Laboratory of Science and Technology on Aerospace Vehicle, Chengdu 610091, China
* Correspondence: ganjh105@buaa.edu.cn

Abstract

Focusing on the vertical return mission scenario of reusable launch vehicles, analytical guidance methods commonly adopted in existing research lack effective fuel prediction mechanisms, which severely restricts the mission reliability and fuel economy of vehicle vertical landing, and fails to achieve high-precision velocity constraint control and stable anti-disturbance guidance in the full powered descent and terminal landing process. To address the above problems, this paper proposes a multi-phase integrated guidance framework that integrates predefined-time time-varying fractional-order sliding mode control and fuel consumption forecasting. A fuel consumption prediction model incorporating potential energy factor, kinetic energy factor and interference factor is constructed to realize full-process fuel demand prediction in the trajectory planning stage, and the proposed guidance scheme achieves high-precision and strong anti-disturbance guidance performance while satisfying strict full-stage velocity constraint requirements. Simulation results show that the proposed method can realize stable and accurate vertical soft landing under diverse disturbance conditions with minor fuel prediction errors. This method addresses the limitations of traditional analytical guidance methods in terms of mission reliability and fuel economy, improves the system robustness of vertical recovery missions, and provides an effective technical reference for precise landing guidance of reusable launch vehicles.

Keywords: guidance law; reusable launch vehicle; fuel consumption prediction; predefined-time fractional-order sliding mode control

Check for updates

Academic Editor: Mingzhe Hou

Received: 14 July 2026
Revised: 8 August 2026
Accepted: 11 August 2026
Published: 16 August 2026

Copyright: © 2026 by the authors. Licensee MDPI, Basel, Switzerland. This article is an open access article distributed under the terms and conditions of the Creative Commons Attribution (CC BY) license.

1. Introduction

Driven by booming commercial aerospace, reusable launch vehicles (RLVs) have attracted extensive research attention thanks to their low operation costs and rapid launch turnaround [1–3]. The recovery technologies of RLV include various approaches such as parachute recovery, parachute-airbag combined recovery, winged horizontal recovery, vertical recovery, and rotor recovery, among other technical approaches [4]. Among these technologies, vertical recovery has been engineeringly applied in rocket recovery missions such as Falcon 9 and New Shepard due to its strong engineering practicality [5–7].

The vertical rocket recovery process can be divided into four sequential segments: attitude adjustment, power deceleration, aerodynamic deceleration, and vertical landing [8]. During the attitude adjustment segment, the vehicle conducts a body flip maneuver to match

the engine's slowdown demands. The purpose of the power deceleration phase is to reduce the dynamic pressure and heat flux of the rocket body before it enters the dense atmosphere, so as to avoid structural damage. The aerodynamic deceleration phase is that the rocket further decelerates using atmospheric resistance to ensure the rocket body reaches the airspace above the predetermined landing site. The vertical landing phase refers to the process of achieving soft landing through precise control by reigniting the engine. The entire recovery process features a complex flight environment and strong uncertain disturbances [9], and must satisfy multiple constraints such as dynamic pressure, heat flux, overload, and fuel reserve. Therefore, the guidance method is a core focus and technical difficulty in RLV research.

Two mainstream vertical recovery control strategies are widely adopted: trajectory optimization schemes and analytical control laws. Trajectory optimization guidance solves the optimal trajectory offline or online based on optimal performance indicators, with typical methods including particle swarm optimization algorithm [8], pseudo spectral approach [10], together with convex optimization schemes [11–13], etc. Reference [14] analyzes return-trajectory mission strategies of vertically-landing reusable launch vehicles covering launch-site return and downrange landing recovery based on the mission performance of propellant-optimal reentry and landing trajectories. Reference [15] adopts the genetic algorithm to propose a powered-descent and landing guidance strategy by optimizing guidance-algorithm gains and target vectors. Reference [16] applies desensitized optimal control (DOC) to the computationally intensive benchmark problem of rocket descent and landing to speed up computation without losing precision. Reference [17] combines the Gauss pseudospectral method and sequential convex optimization to propose a guidance scheme for high-precision landing and fuel-consumption optimization of reusable launch vehicles. Offline trajectory optimization relies on pre-planned nominal trajectories, which are mostly used in deep space exploration missions such as lunar and Mars exploration [18,19]. It has limited anti-interference ability and insufficient robustness in the complex atmospheric environment of the Earth. Although online trajectory optimization has stronger adaptive ability, it involves heavy computational load and may fail to find feasible solutions, leading to uncontrollable flight trajectories. Analytical guidance obtains the explicit expression of the control quantity through mathematical derivation, including polynomial guidance, gravity turn guidance, and sliding mode guidance. Polynomial guidance converts the landing trajectory into a time-related polynomial. It is simple in design and easy to engineer, but has weak anti-interference ability and is difficult to balance energy optimality [20]. Gravity turn control law nullifies aerodynamic attitude errors including attack angle and sideslip angle, aligning the reverse direction of thrust with flight velocity vector [21]. It features simple attitude control but is significantly affected by the atmospheric environment and cannot achieve high-precision vertical landing. Sliding mode guidance (SMG) ensures the convergence of system state errors by designing a reasonable sliding mode function. It has strong robustness and excellent anti-interference performance, making it more suitable for complex RLV recovery scenarios [22].

Sliding mode control (SMC) gains extensive usage within aerospace vehicle flight control domains. Reference [23] proposes a sliding mode guidance law for the gliding phase of RLV, which can quickly solve guidance commands and adjust lateral distance and velocity dissipation online. Reference [24] designs a flight path following control strategy built upon SMC, which reduces model dependence and improves robustness to atmospheric density and aerodynamic parameter perturbations. Reference [25] develops a unified flight control framework utilizing nonsingular terminal SMC, which realizes finite-time stabilization of terminal attack angle and strengthens disturbance rejection performance. Over the past decade, fractional-order sliding mode control (FOSMC) integrated with fractional calculus

theory has gained widespread research interest, as such approaches surpass traditional integer-order counterparts via faster dynamic responses and improved overall robustness.

Reference [26] constructs a FOSMC strategy with terminal angle limitations and verifies that it exhibits stronger anti-disturbance ability than the integer-order guidance law. Reference [27] puts forward a predefined-time FOSMC and verifies its validity, and this controller exhibits better anti-disturbance performance than integer-order counterparts. The above methods can provide technical support for the guidance of the rocket aerodynamic deceleration phase, but they are difficult to adapt to the requirements of the full vertical recovery guidance process.

Currently, SpaceX's Falcon 9 relies on abundant flight tests to tune guidance parameters. Its trajectory is passively adjusted by real-time sensor feedback throughout the landing phase. Without a pre-set fuel-prediction module, considerable fuel redundancy has to be reserved, which reduces payload capacity. While Blue Origin's New-Glenn heavy-duty reusable booster boasts a steady recovery success rate, it cannot realize advance prediction for multi-engine thrust coordination and deceleration-phase fuel consumption. Flight tests have revealed flaws in phase time-sequence matching and control accuracy of terminal-landing velocity. Meanwhile, Europe's CALLISTO vertical-return demonstrator and domestic reusable launch-vehicle prototypes including the Long March-10B, Zhuque-3 and Long March-12-A face shared technical drawbacks. The powered deceleration, aerodynamic deceleration and vertical-landing phases are designed independently. No multi-phase integrated guidance architecture is available to forecast full-range fuel consumption in the trajectory-planning stage. Multiple ignitions and thrust modulation of the terminal-stage engine are vulnerable to atmospheric turbulence disturbances.

Combined with the deficiencies in existing academic research and practical bottlenecks of engineering equipment, the traditional decentralized guidance scheme lacks a fuel-consumption prediction link, suffers from inconsistent multi-phase guidance strategies and limited control precision of velocity constraints under severe external disturbances. There are two key problems to be solved in the existing sliding mode guidance in the field of RLV vertical recovery. One is that most existing methods can only be applied to the guidance of the aerodynamic deceleration phase and trajectory tracking. They cannot meet the velocity constraints for high-precision velocity control in the power deceleration and vertical landing phases, making it impossible to achieve vertical soft landing. The other is that the fuel constraint problem has not been effectively solved [14]. Existing methods are difficult to predict fuel consumption in advance, which may easily lead to insufficient or excessive remaining fuel, affecting the safety and economy of the recovery mission.

This paper proposes a FOSMC guidance method focusing on the key processes of RLV vertical recovery to address the above problems. The main innovations are as follows:

1. A predefined-time fractional-order sliding mode guidance method is proposed for the full vertical recovery process of reusable launch vehicles. Different from existing methods that only focus on aerodynamic deceleration stage tracking, this method realizes high-precision velocity and terminal angle constraint control throughout all recovery phases, ensuring reliable vertical soft landing under external disturbances.
2. A novel three-factor fuel consumption prediction model containing potential energy, kinetic energy and anti-disturbance factors is established. It quantifies the fuel consumption characteristics caused by energy variation and external disturbances, realizes accurate advance prediction of fuel demand, and solves the fuel surplus and shortage problems of traditional guidance schemes.
3. A multi-phase integrated guidance framework integrating fuel prediction and sliding mode control is constructed. It breaks through the limitation of traditional segmented independent guidance design, realizes full-process coordinated optimization of con-

trol parameters, and effectively improves the landing anti-interference robustness and fuel utilization economy of reusable launch vehicles.

The remaining parts of this paper are organized as follows: In Section 2, sliding mode control methods are proposed for velocity constraints and the guidance process, respectively, and the proof of stability and convergence is completed. In Section 3, sliding mode guidance laws are designed for the three phases, namely the power deceleration phase, aerodynamic deceleration phase, and vertical landing phase, respectively. In Section 4, a fuel consumption prediction model is proposed, and the influence mechanism of potential energy, kinetic energy, and uncertain disturbances on fuel consumption is analyzed. In Section 5, the applicability and robustness of the proposed method are verified through four sets of simulation examples. Section 6 presents the conclusions of the full paper.

2. Preliminaries

This paper focuses on establishing a hierarchical sliding-mode control framework, in which the guidance problem for rocket vertical recovery is decomposed into a first-order velocity control system and a second-order nonlinear guidance system: the first-order system performs high-precision velocity braking control to satisfy terminal velocity constraints at each phase, while the second-order system addresses position deviation and attitude angle control to fulfill precise terminal position and angle constraints. In this section, two predefined-time FOSMC are separately designed for the first-order and second-order systems with the goal of providing a robust and disturbance-rejection sliding-mode guidance law for the three phases of powered deceleration, aerodynamic deceleration, and vertical landing in the subsequent section, thereby achieving reliable and precise vertical soft landing under full-range mission constraints.

2.1. Predefined-Time FOSMC for a First-Order Nonlinear System

A first-order nonlinear system with uncertain disturbances is expressed as follows.

$$\chi' = F(\chi, t) + G(\chi, t)u(t) + \Delta(t) \tag{1}$$

In the above formula, χ denotes the system state, $F(\chi, t)$ and $G(\chi, t)$ stand for nonlinear mapping terms, $u(t)$ represents the control input, and $\Delta(t)$ refers to unknown external perturbations. This paper constructs a predefined-time FOSMC defined below.

$$S_1 = e_1 e^{a\left(t_{f1}-t\right)^{p_1}/\left(t_{f1}-t_0\right)^{p_1}} + C_1\left(t_{f1}-t\right)^{q_1}/\left(t_{f1}-t_0\right)^{q_1} \tag{2}$$

where a, p_1 and q_1 correspond to fixed positive gain parameters, t_0 stands for the starting moment, t_{f1} denotes the user-defined convergence duration, $e_1 = \chi - \chi_c$, χ_c is the expected state, C_1 denotes a fixed parameter solved from initial constraints, and its value satisfies $C_1 = -e_1(t_0)e^a$.

The primary time derivative of the sliding surface formulated in Equation (2) is

$$\begin{aligned} S'_1 =& e'_1 e^{a\left(t_{f1}-t\right)^{p_1}/\left(t_{f1}-t_0\right)^{p_1}} - ap_1 e_1 e^{a\left(t_{f1}-t\right)^{p_1}/\left(t_{f1}-t_0\right)^{p_1}}\left(t_{f1}-t\right)^{p_1-1}/\left(t_{f1}-t_0\right)^{p_1} - \\ & C_1 q_1\left(t_{f1}-t\right)^{q_1-1}/\left(t_{f1}-t_0\right)^{q_1} \end{aligned} \tag{3}$$

From Equation (3), the equivalent control quantity u_{eq} can be obtained

$$u_{eq}(t) = \frac{1}{G(\chi,t)}\left(\chi'_c - F(\chi,t) + ap_1e_1\left(t_{f1}-t\right)^{p_1-1}/\left(t_{f1}-t_0\right)^{p_1} + C_1q_1\left(t_{f1}-t\right)^{q_1-1}/\left(\left(t_{f1}-t_0\right)^{q_1}e^{a\left(t_{f1}-t\right)^{p_1}/\left(t_{f1}-t_0\right)^{p_1}}\right)\right) \tag{4}$$

The switching control quantity u_{sw} offsets compound interferences stemming from parametric drift and outside perturbations.

$$u_{sw}(t) = -\frac{K_1\mathrm{sgn}(S_1)}{G(\chi,t)} \tag{5}$$

where K_1 is the switching gain coefficient, and $K_1 > d(t)$.

Combined with Equations (4) and (5), the predefined-time FOSMC is designed as

$$u(t) = \frac{1}{G(\chi,t)}\left(\chi'_c - F(\chi,t) + ap_1e_1\left(t_{f1}-t\right)^{p_1-1}/\left(t_{f1}-t_0\right)^{p_1} + C_1q_1\left(t_{f1}-t\right)^{q_1-1}/\left(\left(t_{f1}-t_0\right)^{q_1}e^{a\left(t_{f1}-t\right)^{p_1}/\left(t_{f1}-t_0\right)^{p_1}}\right) - K_1\mathrm{sgn}(S_1)\right) \tag{6}$$

Theorem 1. *Considering the first-order nonlinear system described by Equation (1), this study adopts a predefined-time FOSMC scheme in (6) and derives the conclusions below.*

(1). The system is stable with global robustness.

(2). The system realizes predefined-time stabilization, whose state variables converge to target reference values exactly at the designated instant t_f.

Proof of Theorem 1. The stability of the single-order variable-structure control system is verified utilizing Lyapunov's stability criterion. A positive-definite Lyapunov candidate function is constructed as

$$V_1 = \frac{1}{2}S_1^2 \tag{7}$$

The first derivative of V_1 is

$$\begin{aligned} V'_1 &= S_1S'_1 \\ &= S_1\Big(\left(F(\chi,t)+G(\chi,t)u(t)+\Delta(t)-\chi'_c\right)e^{a\left(t_{f1}-t\right)^{p_1}/\left(t_{f1}-t_0\right)^{p_1}} - \\ &ap_1e_1e^{a\left(t_{f1}-t\right)^{p_1}/\left(t_{f1}-t_0\right)^{p_1}}\left(t_{f1}-t\right)^{p_1-1}/\left(t_{f1}-t_0\right)^{p_1} - C_1q_1\left(t_{f1}-t\right)^{q_1-1}/\left(t_{f1}-t_0\right)^{q_1}\Big) \\ &= S_1(\Delta(t)-K_1\mathrm{sgn}(S_1))e^{a\left(t_{f1}-t\right)^{p_1}/\left(t_{f1}-t_0\right)^{p_1}} \\ &= (\Delta(t)S_1 - K_1|S_1|)e^{a\left(t_{f1}-t\right)^{p_1}/\left(t_{f1}-t_0\right)^{p_1}} \end{aligned} \tag{8}$$

$V'_1 \le 0$ is obtained from Equation (8), and "=" is taken only if $S_1 = 0$, which can thus be concluded that the system maintains stable operation.

When $t = t_0$, $S_1(t_0) = 0$ can be obtained from Equation (2) and $C_1 = -e_1(t_0)e^a$, that is, $V_1(S_1(t_0)) = 0$. From $V'_1 \le 0$, one can get $V_1 \le 0$. Because of $V_1 = \frac{1}{2}S_1^2 \ge 0$. Thus, $S_1 \equiv 0$ satisfies the global sliding mode, which implies that the system possesses global robustness.

From $S_1 \equiv 0$, the following equation can be obtained from Equation (2).

$$e_1e^{a\left(t_{f1}-t\right)^{p_1}/\left(t_{f1}-t_0\right)^{p_1}} + C_1\left(t_{f1}-t\right)^{q_1}/\left(t_{f1}-t_0\right)^{q_1} = 0 \tag{9}$$

The analytical formula of e_1 can be obtained by solving Equation (9).

$$e_1 = -C_1\left(t_f - t\right)^q / \left(\left(t_f - t_0\right)^q e^{a\left(t_f - t\right)^p / \left(t_f - t_0\right)^p}\right) \tag{10}$$

When $t = t_f$, one can get $e_1 = 0$, which guarantees all state variables approach reference targets, so the system realizes predefined-time stabilization performance.

□

2.2. Predefined-Time FOSMC for a Second-Order Nonlinear System

The following second-order nonlinear system with unknown disturbances is expressed as follows.

$$\begin{cases} x'_1 = \chi_2 \\ x'_2 = F(x,t) + G(x,t)u(t) + \Delta(t) \end{cases} \tag{11}$$

where $x = [x_1, x_2]^T$ denote the system states, $F(x,t)$ and $G(x,t)$ stand for nonlinear mapping terms, $u(t)$ represents the control input, $\Delta(t)$ refers to unknown external perturbations.

For an intuitive explanation of fractional calculus theories, fractional differentiation and integration mathematical definitions and two lemmas are given in sequence below.

Definition 1. *Given a positive integer N and real number λ satisfying $0 \le N-1 \le \lambda < N$, the fractional derivative corresponding to the function $f(t)$ is defined as [28]*

$${}_{t_0}\mathcal{D}_t^{\lambda} f(t) = \frac{1}{\Gamma(n-\lambda)} \int_{t_0}^{t} \frac{f^{(n)}(\tau)}{(t-\tau)^{1+\lambda-n}} d\tau \tag{12}$$

where $\Gamma(\lambda) = \int_0^{\infty} e^{-t} t^{\lambda-1} dt$ is the Gamma function.

Definition 2. *The expression for fractional integration of $f(t)$ can be summarized by the following formula [29].*

$${}_{t_0}\mathcal{D}_t^{\lambda} f(t) = \frac{1}{\Gamma(-\lambda)} \int_{t_0}^{t} \frac{f(\tau)}{(t-\tau)^{1+\lambda}} d\tau \tag{13}$$

where $\lambda < 0$ and $\lambda \in R$.

Lemma 1. *When $f(t)$ remains continuous within $[t_0, \infty)$, a point $\sigma \in (t_0, t)$ exists for each $[t_0, \infty)$ and Equation (22) holds [30]*

$${}_{t_0}D_t^{\lambda} f(t) = f(\sigma) \frac{(t-t_0)^{-\lambda}}{\Gamma(1-\lambda)} \tag{14}$$

here $\lambda \in \mathbb{R}$ and it satisfies $\lambda < 0$.

Lemma 2. *For an integer-valued parameter n, the fractional-order derivative relation given below is valid [31]*

$$\frac{d^n}{dt^n}\left[{}_{t_0}\mathcal{D}_t^{\lambda} f(t)\right] = {}_{t_0}\mathcal{D}_t^{\lambda}\left[\frac{d^n}{dt^n} f(t)\right]. \tag{15}$$

For the foregoing second-order model, a sliding function of predefined-time FOSMC is constructed as follows.

$$S_2 = e_2 + \frac{n e_1}{\left(t_f - t\right)} + C_2 \frac{\left(t_f - t\right)^m}{\left(t_f - t_0\right)^m} + F \frac{\left(t_f - t\right)^n}{\left(t_f - t_0\right)^n} {}_{t_0}\mathcal{D}_t^{\lambda} e_1 \tag{16}$$

where n, F and m are constant gain coefficients, $e_2 = e'_1$, $e_1 = x_1 - x_{1c}$, $e_2 = x_2 - x_{2c}$, x_{1c} and x_{2c} are expected states, e_1 and e_2 represent tracking errors, t_0 denotes the system initial instant, while t_f represents the manually preset convergence moment, $F_{t_0}\mathcal{D}_t^{\lambda}e_1\left(t_f - t\right)^n / \left(t_f - t_0\right)^n$ is the fractional order term, $\lambda \in R$, $\lambda \neq 0$, $C_2 = -\left(e_2(t_0) + ne_1(t_0) / \left(t_f - t_0\right)\right)$ is the time-variant gain coefficient determined from initial system states.

The first derivative of S_2 is obtainable via the calculation in Equation (16).

$$\begin{aligned} S'_2 =& e'_2 + \frac{ne_2}{\left(t_f - t\right)} + \frac{ne_1}{\left(t_f - t\right)^2} - C_2 m \frac{\left(t_f - t\right)^{m-1}}{\left(t_f - t_0\right)^m} - Fn \frac{\left(t_f - t\right)^{n-1}}{\left(t_f - t_0\right)^n} {}_{t_0}\mathcal{D}_t^{\lambda} e_1 + \\ & F \frac{\left(t_f - t\right)^n}{\left(t_f - t_0\right)^n} {}_{t_0}\mathcal{D}_t^{\lambda+1} e_1 \end{aligned} \tag{17}$$

From Equation (17), the equivalent control quantity u_{eq} can be obtained

$$\begin{aligned} u_{eq} =& \frac{1}{G(x,t)} \left(x'_{2c} - F(\mathbf{x}, t) - \frac{ne_2}{\left(t_f - t\right)} - \frac{ne_1}{\left(t_f - t\right)^2} + C_2 m \frac{\left(t_f - t\right)^{m-1}}{\left(t_f - t_0\right)^m} + \right. \\ & \left. Fn \frac{\left(t_f - t\right)^{n-1}}{\left(t_f - t_0\right)^n} {}_{t_0}\mathcal{D}_t^{\lambda} e_1 - F \frac{\left(t_f - t\right)^n}{\left(t_f - t_0\right)^n} {}_{t_0}\mathcal{D}_t^{\lambda+1} e_1 \right) \end{aligned} \tag{18}$$

The switching control quantity u_{sw} is

$$u_{sw}(t) = -\frac{K_2 \mathrm{sgn}(S_2)}{G(x,t)} \tag{19}$$

Combining Equation (18) and (19), the predefined-time FOSMC can be obtained

$$\begin{aligned} u_{eq} =& \frac{1}{G(x,t)} \left(x'_{2c} - F(\mathbf{x}, t) - \frac{ne_2}{\left(t_f - t\right)} - \frac{ne_1}{\left(t_f - t\right)^2} + C_2 m \frac{\left(t_f - t\right)^{m-1}}{\left(t_f - t_0\right)^m} + \right. \\ & \left. Fn \frac{\left(t_f - t\right)^{n-1}}{\left(t_f - t_0\right)^n} {}_{t_0}\mathcal{D}_t^{\lambda} e_1 - F \frac{\left(t_f - t\right)^n}{\left(t_f - t_0\right)^n} {}_{t_0}\mathcal{D}_t^{\lambda+1} e_1 - K_2 \mathrm{sgn}(S_2) \right) \end{aligned} \tag{20}$$

Theorem 2. *Considering the second-order nonlinear system described by Equation (11), this study adopts a predefined-time FOSMC scheme in (20) and derives the conclusions below.*

(1). The system is stable with global robustness.

(2). The system realizes predefined-time stabilization, whose state variables converge to target reference values exactly at the designated instant t_f.

Proof of Theorem 2. The positive-definite Lyapunov candidate function is constructed as

$$V_2 = \frac{1}{2} S_2^2 \tag{21}$$

The first derivative of V_2 is

$$\begin{aligned} V_2' =& S_2 S_2' \\ &= S_2\Big(F(x,t) + G(x,t)u(t) + d(t) - x_{2c}' + \frac{ne_2}{(t_f - t)} + \frac{ne_1}{(t_f - t)^2} \\ &\quad - C_2 m\frac{(t_f - t)^{m-1}}{(t_f - t_0)^m} - Fn\frac{(t_f - t)^{n-1}}{(t_f - t_0)^n}{}_{t_0}\mathcal{D}_t^{\lambda} e_1 + F\frac{(t_f - t)^n}{(t_f - t_0)^n}{}_{t_0}\mathcal{D}_t^{\lambda+1} e_1\Big) \\ &= d(t)S_2 - K_2|S_2| \end{aligned} \tag{22}$$

From Equation (22), one can get $V_2' \leq 0$, and "=" is taken only if $S_2 = 0$, which validates the stable operation of the dynamic system.

When $t = t_0$, it yields

$$\begin{aligned} |S_2(t_0)| &= \left|e_2(t_0) + \frac{ne_1(t_0)}{t_f - t_0} + C_2 + F_{t_0}\mathcal{D}_{t_0}^{\lambda} e_1(t_0)\right| \\ &= \left|F_{t_0}\mathcal{D}_{t_0}^{\lambda} e_1(t_0)\right| \\ &= \begin{cases} \left|\lim\limits_{t\to t_0} \frac{F}{\Gamma(-\lambda)} \int_{t_0}^{t} \frac{e_1(\tau)}{(t-\tau)^{1+\lambda}} d\tau\right| \leq \frac{F|e_1(\tau)|_{\max}}{-\lambda\Gamma(-\lambda)} \lim\limits_{t\to t_0} (t - t_0)^{-\lambda} = 0, \lambda < 0 \\ \left|\lim\limits_{t\to t_0} \frac{F}{\Gamma(N-\lambda)} \int_{t_0}^{t} \frac{{e_1}^N(\tau)}{(t-\tau)^{1+\lambda-N}} d\tau\right| \leq \frac{F\left|{e_1}^N(\tau)\right|_{\max} \lim\limits_{t\to t_0} (t-t_0)^{N-\lambda}}{(N-\lambda)\Gamma(N-\lambda)} = 0, \lambda > 0 \end{cases} \end{aligned} \tag{23}$$

where N is a positive integer and $0 \leq N - 1 \leq \lambda < N$.

According Equation (23), $S_2(t_0) = 0$ can be obtained, which means $V_2(S_2(t_0)) = 0$, and it yields $V_2 \leq 0$ from Equation (22). One can get that $V_2 = \frac{1}{2}S_2^2 \geq 0$. Thus, $S_2 \equiv 0$ and the designed system fulfills the requirements of global sliding mode motion, which implies that the system possesses global robustness.

Subsequently, rigorous proof is provided to validate the system's predefined-time convergence property.

When $\lambda < 0$, according to the fractional-order mean value theorem shown in Lemma 1, for $\forall t \in [t_0, \infty)$, there is at least one point $\xi_1 \in (t_0, t)$ that the subsequent equality can be obtained

$$F\frac{(t_f - t)^n}{(t_f - t_0)^n}{}_{t_0}\mathcal{D}_t^{\lambda} e_1 = Fe_1(\xi_1)\frac{(t_f - t)^n (t - t_0)^{-\lambda}}{(t_f - t_0)^n \Gamma(1 - \lambda)} \tag{24}$$

When $S_2 = 0$, Equation (25) is derived from Equations (14) and (24).

$$e_2 + \frac{n}{t_f - t} e_1 = -C_2\frac{(t_f - t)^m}{(t_f - t_0)^m} - Fe_1(\xi_1)\frac{(t_f - t)^n (t - t_0)^{-\lambda}}{(t_f - t_0)^n \Gamma(1 - \lambda)} \tag{25}$$

By solving Equation (25), the analytical formula of e_1 can be obtained as

$$e_1 = C_e(t_f - t)^n + \frac{C_2(t_f - t)^{m+1}}{(m - n + 1)(t_f - t_0)^m} - \frac{Fe_1(\xi_1)(t_f - t)^n (t - t_0)^{1-\lambda}}{(1 - \lambda)\Gamma(1 - \lambda)(t_f - t_0)^n} \tag{26}$$

where C_e stands for a constant parameter calculated from initial-state constraints.

$$C_e = \frac{e_1(t_0)}{(t_f - t_0)^n} - \frac{C_2(t_f - t_0)^{1-n}}{m - n + 1} \tag{27}$$

Calculating the first-order differential of e_1 yields the analytical formula of e_2.

$$\begin{aligned} e_2 = &- nC_e(t_f - t)^{n-1} - \frac{(m+1)C_2(t_f - t)^m}{(m-n+1)(t_f - t_0)^m} - \frac{Fe_1(\xi_1)(t_f - t)^n(t - t_0)^{-\lambda}}{\Gamma(1-\lambda)(t_f - t_0)^n} \\ &+ \frac{nFe_1(\xi_1)(t_f - t)^{n-1}(t - t_0)^{1-\lambda}}{(1-\lambda)\Gamma(1-\lambda)(t_f - t_0)^n} \end{aligned} \tag{28}$$

For $\lambda > 0$, it can be concluded from Lemma 1 and Lemma 2 that for arbitrary $\forall t \in [t_0, \infty)$, a point $\xi_2 \in (t_0, t)$ exists to satisfy the equation below.

$$F\frac{(t_f - t)^n}{(t_f - t_0)^n}{}_{t_0}\mathcal{D}_t^{\lambda} e_1 = F\frac{(t_f - t)^n}{(t_f - t_0)^n}{}_{t_0}\mathcal{D}_t^{\lambda - N} e_1^{(N)} = Fe_1^{(N)}(\xi_2)\frac{(t_f - t)^n(t - t_0)^{N-\lambda}}{(t_f - t_0)^n\Gamma(1+N-\lambda)} \tag{29}$$

in which a positive integer N is defined such that $0 \leq N - 1 \leq \lambda < N$.

When $S_2 = 0$, Equation (30) is derived from Equations (14) and (29)

$$e_2 + \frac{n}{t_f - t}e_1 = -C_2\frac{(t_f - t)^m}{(t_f - t_0)^m} - Fe_1^{(N)}(\xi_2)\frac{(t_f - t)^n(t - t_0)^{N-\lambda}}{(t_f - t_0)^n\Gamma(1+N-\lambda)} \tag{30}$$

Similarly, one can get the analytical formula of e_1 and e_2 as

$$e_1 = C_e(t_f - t)^n + \frac{C_2(t_f - t)^{m+1}}{(m-n+1)(t_f - t_0)^m} - \frac{Fe_1^{(N)}(\xi_2)(t_f - t)^n(t - t_0)^{1+N-\lambda}}{(1+N-\lambda)\Gamma(1+N-\lambda)(t_f - t_0)^n} \tag{31}$$

$$\begin{aligned} e_2 = &- nC_e(t_f - t)^{n-1} - \frac{(m+1)C_2(t_f - t)^m}{(m-n+1)(t_f - t_0)^m} - \frac{Fe_1^{(N)}(\xi_2)(t_f - t)^n(t - t_0)^{N-\lambda}}{\Gamma(1+N-\lambda)(t_f - t_0)^n} \\ &+ \frac{nFe_1^{(N)}(\xi_2)(t_f - t)^{n-1}(t - t_0)^{1+N-\lambda}}{(1+N-\lambda)\Gamma(1+N-\lambda)(t_f - t_0)^n} \end{aligned} \tag{32}$$

According to Equations (26), (28), (31) and (32), when $t = t_f$, the state errors e_1 and e_2 decay to zero subject to $m - n + 1 \neq 0$, $m > 0$ and $n > 1$, indicates that the control system can achieve arbitrary-time convergence. □

3. Guidance Law Design

3.1. Dynamic Model

In this part, fractional-order time-varying sliding mode guidance (FOTSMG) strategies are constructed for the powered-deceleration stage, aerodynamic-deceleration stage and vertical-landing stage during rocket recovery, to achieve precise vertical soft landing while satisfying dynamic pressure constraints, load factor constraints, engine flow constraints, and fuel constraints. The guidance process is depicted in Figure 1.

As shown in Figure 1, the upper part corresponds to the powered deceleration phase, the middle region denotes the aerodynamic deceleration phase, and the bottom part represents the vertical landing phase. y_0 and v_0 represent the initial altitude and velocity, respectively, at the start of the powered deceleration phase. y_{f1} and v_{f1} denote the minimum altitude and terminal velocity, respectively, for the powered deceleration phase. y_{f2} and v_{f2} correspond to the minimum altitude and terminal velocity, respectively, of the aerodynamic deceleration phase. y_{f3} and v_{f3} are landing altitude and landing speed of the launch vehicle, respectively. In the powered deceleration phase, the rocket engine generates reverse thrust to reduce velocity. This active braking limits the dynamic pressure and aerodynamic heat flux before the vehicle enters the dense atmosphere, preventing structural damage caused by excessive thermal and aerodynamic loads. During the aerody-

namic deceleration phase, the vehicle relies on atmospheric drag to further dissipate kinetic energy and slow down. Meanwhile, the guidance system continuously adjusts the flight trajectory to steer the vehicle to the designated airspace directly above the pre-planned landing site. For the vertical landing phase, the main engine is reignited to provide braking thrust. Closed-loop guidance control is adopted to eliminate residual descent velocity, enabling precise and gentle vertical soft landing.

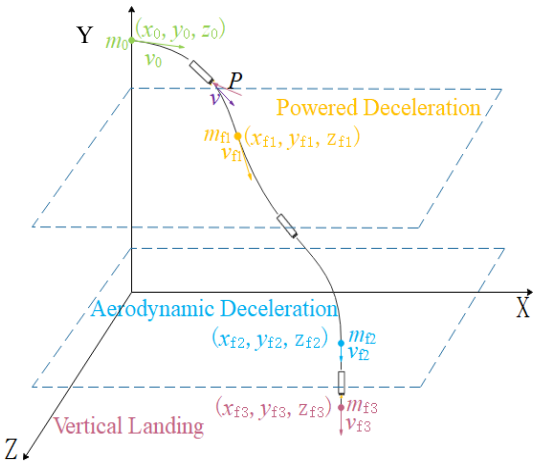


Figure 1. Rocket recovery terminal guidance process.

The following formulas describe the three-dimensional kinematics and dynamics of the rocket.

$$\dot{x} = v\cos\gamma\cos\chi \tag{33}$$

$$\dot{y} = v\sin\gamma \tag{34}$$

$$\dot{z} = -v\cos\gamma\sin\chi \tag{35}$$

$$\dot{v} = \frac{-D - mg\sin\gamma - P_1 - F_{ex} - F_{kx}}{m} + d_{w1} \tag{36}$$

$$\dot{\gamma} = \frac{L\cos\mu - mg\cos\gamma - P_2 - F_{ey} - F_{ky}}{mv} + d_{w2} \tag{37}$$

$$\dot{\chi} = -\frac{L\sin\mu - P_3 - F_{ez} - F_{kz}}{mv\cos\gamma} + d_{w3} \tag{38}$$

$$\dot{m} = -\frac{P}{I_{sg}} \tag{39}$$

here, v, γ, χ, m, g, α, μ, I_{sg}, D, L represent the flight velocity, flight path angle, trajectory deflection angle, rocket mass, gravitational acceleration, angle of attack, roll angle, the engine specific impulse, the aerodynamic resistance, the aerodynamic lift, respectively. $\boldsymbol{F}_e = [F_{ex}, F_{ey}, \boldsymbol{F}_{ez}]^{\mathrm{T}}$ is the centrifugal inertia force, $\boldsymbol{F}_k = [F_{kx}, F_{ky}, F_{kz}]^{\mathrm{T}}$ is the Coriolis inertia force, $\boldsymbol{d}_w = [d_{w1}, d_{w2}, d_{w3}]^{\mathrm{T}}$ is uncertain disturbances and $\boldsymbol{P}_T = [P_1, P_2, P_3]^{\mathrm{T}}$ is the engine thrust.

$$\begin{cases} \boldsymbol{F}_e = 2m\boldsymbol{\omega}_e \times \boldsymbol{v} \\ \boldsymbol{F}_k = m\boldsymbol{\omega}_e \times (\boldsymbol{\omega}_e \times \boldsymbol{r}) \end{cases} \tag{40}$$

$$\boldsymbol{P}_T = \begin{bmatrix} \cos\alpha & -\sin\alpha & 0 \\ \sin\alpha\cos\mu & \cos\alpha\cos\mu & -\sin\mu \\ \sin\alpha\sin\mu & \cos\alpha\sin\mu & \cos\mu \end{bmatrix} \begin{bmatrix} P\cos\varphi \\ P\sin\varphi\cos\psi \\ P\sin\varphi\sin\psi \end{bmatrix} \tag{41}$$

where $\boldsymbol{\omega}_e$ denotes the Earth's rotation speed vector, $\boldsymbol{v}$ represents the rocket velocity vector, $\boldsymbol{r}$ denotes the position vector pointing from the geocenter to the centroid of the rocket.

In addition, $|\boldsymbol{r}| = R_0 + y$, where R_0 stands for the Earth's radius. P is the engine thrust value, φ and ψ are engine deflection angles, as shown in Figure 2. The solid purple line equipped with an arrow denotes the engine-generated thrust, where the arrow points out the thrust direction. The orange arrow-marked line refers to the projection of engine thrust upon the X_bZ_b plane.

It is difficult to accurately control the time in the guidance process, so this paper uses the pseudo altitude variable τ instead of the time variable t to set the guidance law. Let the pseudo height variable τ be

$$\tau = y_0 - y \tag{42}$$

where y_0 is the initial altitude of the aircraft and y is the altitude of the aircraft at the current time. The relationship between time variable t and pseudo height variable τ is

$$t' = \frac{\mathrm{d}t}{\mathrm{d}\tau} = -\frac{1}{v\sin\gamma} \tag{43}$$

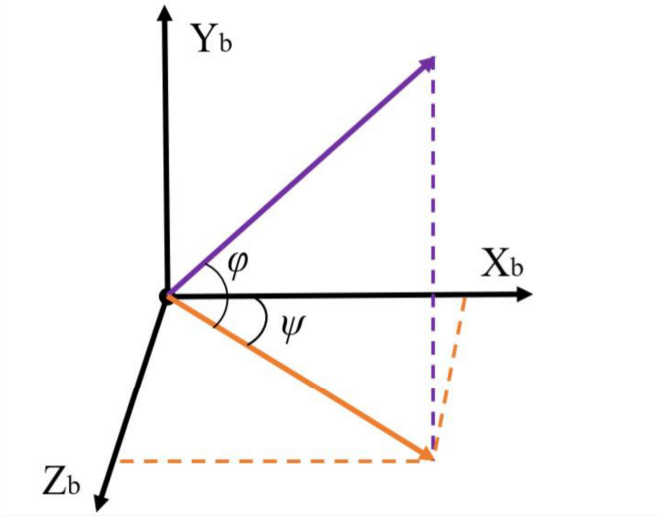


Figure 2. Engine thrust in missile body coordinate system.

Therefore, Equations (33)–(39) can be transformed into the following equations with the pseudo height variable τ as the independent variable

$$x' = \frac{\mathrm{d}x}{\mathrm{d}\tau} = \frac{\mathrm{d}x}{\mathrm{d}t}\frac{\mathrm{d}t}{\mathrm{d}\tau} = -\cot\gamma\cos\chi \tag{44}$$

$$y' = \frac{\mathrm{d}y}{\mathrm{d}\tau} = -1 \tag{45}$$

$$z' = \cot\gamma\sin\chi \tag{46}$$

$$v' = \frac{\mathrm{d}v}{\mathrm{d}\tau} = \frac{\mathrm{d}v}{\mathrm{d}t}\frac{\mathrm{d}t}{\mathrm{d}\tau} = \frac{D + mg\sin\gamma + P_1 + F_{ex} + F_{kx}}{mv\sin\gamma} - \frac{d_{w1}}{v\sin\gamma} \tag{47}$$

$$\gamma' = \frac{\mathrm{d}\gamma}{\mathrm{d}\tau} = \frac{\mathrm{d}\gamma}{\mathrm{d}t}\frac{\mathrm{d}t}{\mathrm{d}\tau} = \frac{-L\cos\mu + mg\cos\gamma + P_2 + F_{ey} + F_{ky}}{mv^2\sin\gamma} - \frac{d_{w2}}{v\sin\gamma} \tag{48}$$

$$\chi' = \frac{\mathrm{d}\chi}{\mathrm{d}\tau} = \frac{\mathrm{d}\chi}{\mathrm{d}t}\frac{\mathrm{d}t}{\mathrm{d}\tau} = \frac{L\sin\mu - P_3 - F_{ez} - F_{kz}}{mv^2\cos\gamma\sin\gamma} - \frac{d_{w3}}{v\sin\gamma} \tag{49}$$

$$m' = \frac{dm}{dt}\frac{dt}{d\tau} = \frac{P}{I_{sg}v\sin\gamma} \tag{50}$$

Subsequently, combined with Equations (44)–(50), the FOTSMG is proposed to achieve soft landing by controlling aerodynamic lift L, engine thrust P and engine deflection angle δ.

Remark 1. *In the powered deceleration stage, speed constraints and engine flow constraints need to be taken into account. In the aerodynamic deceleration stage, the rocket mass remains unchanged, and aerodynamic force serves as the main control force of the rocket, which is subject to the constraints of load factor, heat flux and dynamic pressure. In the vertical landing stage, due to the relatively low speed and altitude, the impacts of load factor, heat flux and dynamic pressure constraints on the rocket can be neglected, and only the angle constraints and remaining available fuel constraints need to be considered. Dynamic pressure and heat flux are constrained by regulating the speed, while load factor is constrained by controlling the normal acceleration. The engine mass flow constraint is achieved by limiting the maximum and minimum thrust. The current section primarily addresses FOTSMG law design, and a detailed investigation of residual fuel constraints will be provided in the following section.*

3.2. Powered Deceleration Guidance Law

The pseudo height variation range of the powered deceleration stage is $\tau_0 \sim \tau_{f1}$, and $\tau_{f1} = y_0 - y_{f1}$. In this stage, the maximum dynamic pressure is reduced by reducing the rocket speed to the extent that the grid rudder can bear, and the disintegration of the rocket due to excessive dynamic pressure is avoided. Thin air means low aerodynamic power, which is further reduced by zero angle of attack with the idea of gravity turn guidance. Therefore, the aerodynamic force and inertial force can be regarded as uncertain interference, and Equation (47) can be simplified to

$$v' = \frac{P_1 + mg\sin\gamma}{mv\sin\gamma} + d_1 \tag{51}$$

where $d_1 = \frac{D+F_{ex}+F_{kx}}{mv\sin\gamma} - \frac{d_{w1}}{v\sin\gamma}$.

The state error e_1 is

$$e_1 = v - v_{f1} \tag{52}$$

where v_{f1} is the desired speed of the rocket at altitude y_{f1}, which is used to restrict the maximum dynamic pressure on the rocket in the subsequent aerodynamic deceleration phase.

In this stage, speed control is the focus. Let α, μ, ϕ and ψ be zero, and one can get the following first-order nonlinear system.

$$e_1{}' = v' - v'_{f1} = \frac{P + mg\sin\gamma}{mv\sin\gamma} - v'_{f1} + d_1 \tag{53}$$

The sliding mode function is designed

$$S_1 = e_1 e^{a_1\left(\tau_{f1}-\tau\right)^{p_1}/\left(\tau_{f1}-\tau_0\right)^{p_1}} + C_1\left(\tau_{f1}-\tau\right)^{p_1}/\left(\tau_{f1}-\tau_0\right)^{p_1} \tag{54}$$

where a_1 and p_1 are constant gain positive coefficients, C_1 stands for a constant value relying on the system-initial states, and $C_1 = -e_1(\tau_0)e^{a_1}$.

Based on Theorem 1, one acquires the expression of engine thrust P corresponding to the first-order nonlinear system in Equation (53).

$$\begin{aligned} P = &- mg\sin\gamma + mv\sin\gamma\Bigg(-K_1\mathrm{sgn}(S_1) + a_1p_1e_1\left(\tau_{f1}-\tau\right)^{p_1-1}/\left(\tau_{f1}-\tau_0\right)^{p_1} + \\ &C_1p_1\left(\tau_{f1}-\tau\right)^{p_1-1}/\left(\left(\tau_{f1}-\tau_0\right)^{p_1}e^{a_1\left(\tau_{f1}-\tau\right)^{p_1}/\left(\tau_{f1}-\tau_0\right)^{p_1}}\right)\Bigg) \end{aligned} \tag{55}$$

where K_1 is a constant and $K_1 > |d_1|$.

3.3. Aerodynamic Deceleration Guidance Law

After the powered deceleration phase ends, the rocket enters the aerodynamic deceleration stage. During the aerodynamic deceleration stage, the rocket opens the grille rudder to gain more lift for guidance and resistance for deceleration. The pseudo height variation range of the aerodynamic deceleration section is $\tau_{f1} \sim \tau_{f2}$, and $\tau_{f2} = y_{f1} - y_{f2}$. In this stage, the engine is shut down and the attitude of the rocket is adjusted by the rudder, so as to control the aerodynamic force for guidance.

Taking the inertial force as uncertain interference, Equations (48) and (49) can be simplified to

$$\gamma' = \frac{-L\cos\mu + mg\cos\gamma}{mv^2\sin\gamma} + \hat{d}_{21} \tag{56}$$

$$\chi' = \frac{L\sin\mu}{mv^2\cos\gamma\sin\gamma} + \hat{d}_{22} \tag{57}$$

where $\hat{d}_{21} = \frac{F_{ey}+F_{kz}}{mv^2\sin\gamma} - \frac{d_{w2}}{v\sin\gamma}$ and $\hat{d}_{22} = \frac{-F_{ez}-F_{kz}}{mv^2\cos\gamma\sin\gamma} - \frac{d_{w3}}{v\sin\gamma}$.

In this stage, in addition to reaching the designated landing position, the rocket also needs to meet the landing angle of $-90°$. In order to realize the above terminal requirements, the following four intermediate error variables are designed

$$\begin{cases} \zeta_1 = x - x_f + \left(\tau - \tau_{f2}\right)\cot\gamma_f\cos\chi_f \\ \zeta_2 = \dfrac{d\zeta_1}{d\tau} = x' + \cot\gamma_f\cos\chi_f = \cot\gamma_f\cos\chi_f - \cot\gamma\cos\chi \end{cases} \tag{58}$$

$$\begin{cases} \sigma_1 = z_f - z + \left(\tau - \tau_{f2}\right)\cot\gamma_f\sin\chi_f \\ \sigma_2 = \dfrac{d\sigma_1}{d\tau} = -z' + \cot\gamma_f\sin\chi_f = \cot\gamma_f\sin\chi_f - \cot\gamma\sin\chi \end{cases} \tag{59}$$

where γ_f and χ_f represent the desired terminal flight angles equal to 90°. A second-order nonlinear system with external disturbance uncertainties is constructed from Equations (56)–(59).

$$\begin{cases} \zeta'_1 = \zeta_2 \\ \zeta'_2 = \dfrac{d\zeta_2}{d\tau} = \dfrac{\cos\chi}{\sin^2\gamma}\gamma' + \dfrac{\cos\gamma\sin\chi}{\sin\gamma}\chi' \\ \quad = \dfrac{-L\cos\mu\cos\chi + mg\cos\gamma\cos\chi}{mv^2\sin^3\gamma} + \dfrac{L\sin\mu\cos\gamma\sin\chi}{mv^2\cos\gamma\sin^2\gamma} + d_{21} \end{cases} \tag{60}$$

$$\begin{cases} \sigma'_1 = \sigma_2 \\ \sigma'_2 = \dfrac{d\sigma_2}{d\tau} = \dfrac{\sin\chi}{\sin^2\gamma}\gamma' - \dfrac{\cos\gamma\cos\chi}{\sin\gamma}\chi' \\ \quad = \dfrac{-L\cos\mu\sin\chi + mg\cos\gamma\sin\chi}{mv^2\sin^3\gamma} - \dfrac{L\sin\mu\cos\gamma\cos\chi}{mv^2\cos\gamma\sin^2\gamma} + d_{22} \end{cases} \tag{61}$$

For the above second-order systems, according to the method shown in Section 2.2, the following fractional time-varying sliding mode function can be obtained

$$S_{21} = \zeta_2 + \frac{n_{21}\zeta_1}{\left(\tau_{f2} - \tau\right)} + C_{21}\frac{\left(\tau_{f2} - \tau\right)^{m_{21}}}{\left(\tau_{f2} - \tau_{f1}\right)^{m_{21}}} + F_{21}\frac{\left(\tau_{f2} - \tau\right)^{n_{21}}}{\left(\tau_{f2} - \tau_{f1}\right)^{n_{21}}}{}_{\tau_{f1}}\mathcal{D}_{\tau}^{\lambda_{21}}\zeta_1 \tag{62}$$

$$S_{22} = \sigma_2 + \frac{n_{22}\sigma_1}{\left(\tau_{f2} - \tau\right)} + C_{22}\frac{\left(\tau_{f2} - \tau\right)^{m_{22}}}{\left(\tau_{f2} - \tau_{f1}\right)^{m_{22}}} + F_{22}\frac{\left(\tau_{f2} - \tau\right)^{n_{22}}}{\left(\tau_{f2} - \tau_{f1}\right)^{n_{22}}}\tau_{f1}\mathcal{D}_{\tau}^{\lambda_{22}}\sigma_1 \tag{63}$$

where n_{21}, n_{22}, F_{21}, F_{22}, m_{21} and m_{22} are constant gain coefficients, $n_{21} > 1$, $n_{22} > 1$, $m_{21} > 1$, $m_{22} > 1$, $m_{21} - n_{21} + 1 \neq 0$, $m_{22} - n_{22} + 1 \neq 0$, $\lambda_{21} \in R$, $\lambda_{21} \neq 0$, $\lambda_{22} \in R$, $\lambda_{22} \neq 0$, $C_{21} = -\zeta_2\left(\tau_{f1}\right) - \frac{n_{21}\zeta_1\left(\tau_{f1}\right)}{\left(\tau_{f2} - \tau_{f1}\right)}$ and $C_{22} = -\sigma_2\left(\tau_{f1}\right) - \frac{n_{22}\sigma_1\left(\tau_{f1}\right)}{\left(\tau_{f2} - \tau_{f1}\right)}$.

For the two second-order nonlinear systems given in Equations (60) and (61), by adopting the method presented in Theorem 2, one can get

$$\begin{aligned} L\cos\mu =& mg\cos\gamma + mv^2\sin^3\gamma\left(\cos\chi\left(\frac{n_{21}\zeta_2}{\tau_{f2} - \tau} + \frac{n_{21}\zeta_1}{\left(\tau_{f2} - \tau\right)^2} - \right.\right. \\ & C_{21}m_{21}\frac{\left(\tau_{f2} - \tau\right)^{m_{21}-1}}{\left(\tau_{f2} - \tau_{f1}\right)^{m_{21}}} - n_{21}F_{21}\frac{\left(\tau_{f2} - \tau\right)^{n_{21}-1}}{\left(\tau_{f2} - \tau_{f1}\right)^{n_{21}}}\tau_{f1}\mathcal{D}_{\tau}^{\lambda_{21}}\zeta_1 + \\ & \left.F_{21}\frac{\left(\tau_{f2} - \tau\right)^{n_{21}}}{\left(\tau_{f2} - \tau_{f1}\right)^{n_{21}}}\tau_{f1}\mathcal{D}_{\tau}^{\lambda_{21}+1}\zeta_1 + K_{21}\mathrm{sgn}(S_{21})\right) + \\ & \sin\chi\left(\frac{n_{22}\sigma_2}{\tau_{f2} - \tau} + \frac{n_{22}\sigma_1}{\left(\tau_{f2} - \tau\right)^2} - C_{22}m_{22}\frac{\left(\tau_{f2} - \tau\right)^{m_{22}-1}}{\left(\tau_{f2} - \tau_{f1}\right)^{m_{22}}} + K_{22}\mathrm{sgn}(S_{22}) - \right. \\ & \left.\left.n_{22}F_{22}\frac{\left(\tau_{f2} - \tau\right)^{n_{22}-1}}{\left(\tau_{f2} - \tau_{f1}\right)^{n_{22}}}\tau_{f1}\mathcal{D}_{\tau}^{\lambda_{22}}\zeta_1 + F_{22}\frac{\left(\tau_{f2} - \tau\right)^{n_{22}}}{\left(\tau_{f2} - \tau_{f1}\right)^{n_{22}}}\tau_{f1}\mathcal{D}_{\tau}^{\lambda_{22}+1}\sigma_1\right)\right) \end{aligned} \tag{64}$$

$$\begin{aligned} L\sin\mu =& -mv^2\sin^2\gamma\left(\sin\chi\left(\frac{n_{21}\zeta_2}{\tau_{f2} - \tau} + \frac{n_{21}\zeta_1}{\left(\tau_{f2} - \tau\right)^2} - C_{21}m_{21}\frac{\left(\tau_{f2} - \tau\right)^{m_{21}-1}}{\left(\tau_{f2} - \tau_{f1}\right)^{m_{21}}} - \right.\right. \\ & n_{21}F_{21}\frac{\left(\tau_{f2} - \tau\right)^{n_{21}-1}}{\left(\tau_{f2} - \tau_{f1}\right)^{n_{21}}}\tau_{f1}\mathcal{D}_{\tau}^{\lambda_{21}}\zeta_1 + K_{21}\mathrm{sgn}(S_{21}) \\ & \left.+ F_{21}\frac{\left(\tau_{f2} - \tau\right)^{n_{21}}}{\left(\tau_{f2} - \tau_{f1}\right)^{n_{21}}}\tau_{f1}\mathcal{D}_{\tau}^{\lambda_{21}+1}\zeta_1\right) - \cos\chi\left(\frac{n_{22}\sigma_2}{\tau_{f2} - \tau} + \right. \\ & \frac{n_{22}\sigma_1}{\left(\tau_{f2} - \tau\right)^2} - C_{22}m_{22}\frac{\left(\tau_{f2} - \tau\right)^{m_{22}-1}}{\left(\tau_{f2} - \tau_{f1}\right)^{m_{22}}} + K_{22}\mathrm{sgn}(S_{22}) - \\ & \left.\left.n_{22}F_{22}\frac{\left(\tau_{f2} - \tau\right)^{n_{22}-1}}{\left(\tau_{f2} - \tau_{f1}\right)^{n_{22}}}\tau_{f1}\mathcal{D}_{\tau}^{\lambda_{22}}\zeta_1 + F_{22}\frac{\left(\tau_{f2} - \tau\right)^{n_{22}}}{\left(\tau_{f2} - \tau_{f1}\right)^{n_{22}}}\tau_{f1}\mathcal{D}_{\tau}^{\lambda_{22}+1}\sigma_1\right)\right) \end{aligned} \tag{65}$$

where K_{21} and K_{22} are constants, $K_{21} > d_{21}$ and $K_{22} > d_{22}$. From Equations (64) and (65), the control quantities L and μ can be easily obtained, and the total acceleration is

$$a = \frac{L}{m} \tag{66}$$

3.4. Vertical Landing Guidance Law

At the end of the aerodynamic deceleration stage, the rocket starts the engine for braking deceleration. The final requirement is that when the rocket reaches the landing point, the deviation of position and speed in the horizontal direction is close to zero and the vertical speed is small, through which vertical pinpoint soft-landing for the reusable rocket is fulfilled.

The pseudo height range of the vertical landing section is $\tau_{f2} \sim \tau_{f3}$, and $\tau_{f3} = y_{f2} - y_{f3}$. The aerodynamic forces are smaller during the vertical landing phase when the velocity is small and $\alpha \approx 0$. At this stage, the main control quantities are engine thrust and engine deflection angles, and the torque generated by them is balanced by the small attitude control engine. Regarding aerodynamics and inertial forces as uncertain disturbances, Equations (47)–(49) can be simplified to

$$v' = \frac{P\cos\varphi + mg\sin\gamma}{mv\sin\gamma} + d_{31} \tag{67}$$

$$\gamma' = \frac{P\sin\varphi\cos\psi + mg\cos\gamma}{mv^2\sin\gamma} + \hat{d}_{32} \tag{68}$$

$$\chi' = \frac{-P\sin\varphi\sin\psi}{mv^2\cos\gamma\sin\gamma} + \hat{d}_{33} \tag{69}$$

The five error variables are shown below

$$e_{31} = v - v_{f3} \tag{70}$$

$$\zeta_{31} = x - x_f + \left(\tau - \tau_{f3}\right)\cot\gamma_f\cos\chi_f \tag{71}$$

$$\zeta_{32} = \frac{d\zeta_{31}}{d\tau} = x' + \cot\gamma_f\cos\chi_f = \cot\gamma_f\cos\chi_f - \cot\gamma\cos\chi \tag{72}$$

$$\sigma_{31} = z_f - z + \left(\tau - \tau_{f3}\right)\cot\gamma_f\sin\chi_f \tag{73}$$

$$\sigma_{32} = \frac{d\sigma_{31}}{d\tau} = -z' + \cot\gamma_f\sin\chi_f = \cot\gamma_f\sin\chi_f - \cot\gamma\sin\chi \tag{74}$$

According to Equations (67)–(74), the following first-order and second-order nonlinear systems with uncertain disturbances are obtained

$$e'_{31} = v' - v'_{f3} = \frac{P\cos\varphi + mg\sin\gamma}{mv\sin\gamma} - v'_{f3} + d_{31} \tag{75}$$

$$\begin{cases} \zeta'_{31} = \zeta_{32} \\ \zeta'_{32} = \frac{P\sin\varphi\cos\psi\cos\chi + mg\cos\gamma\cos\chi}{mv^2\sin^3\gamma} + \frac{-P\sin\varphi\sin\psi\cos\gamma\sin\chi}{mv^2\cos\gamma\sin^2\gamma} + d_{32} \end{cases} \tag{76}$$

$$\begin{cases} \sigma'_{31} = \sigma_{32} \\ \sigma'_{32} = \frac{P\sin\varphi\cos\psi\sin\chi + mg\cos\gamma\sin\chi}{mv^2\sin^3\gamma} + \frac{P\sin\varphi\sin\psi\cos\gamma\cos\chi}{mv^2\cos\gamma\sin^2\gamma} + d_{33} \end{cases} \tag{77}$$

For the three nonlinear systems shown in Equations (75)–(77), the sliding mode functions S_{31}, S_{32} and S_{33} are designed as

$$S_{31} = e_{31}e^{a_3\left(\tau_{f3}-\tau\right)^{p_3}/\left(\tau_{f3}-\tau_{f2}\right)^{p_3}} + C_{31}\left(\tau_{f3} - \tau\right)^{p_3}/\left(\tau_{f3} - \tau_{f2}\right)^{p_3} \tag{78}$$

$$S_{32} = \zeta_{32} + \frac{n_{32}\zeta_{31}}{\left(\tau_{f3} - \tau\right)} + C_{32}\frac{\left(\tau_{f3} - \tau\right)^{m_{32}}}{\left(\tau_{f3} - \tau_{f2}\right)^{m_{32}}} + F_{32}\frac{\left(\tau_{f3} - \tau\right)^{n_{32}}}{\left(\tau_{f3} - \tau_{f2}\right)^{n_{32}}}\tau_{f2}\mathcal{D}_\tau^{\lambda_{32}}\zeta_{31} \tag{79}$$

$$S_{33} = \sigma_{32} + \frac{n_{33}\sigma_{31}}{\left(\tau_{f3} - \tau\right)} + C_{33}\frac{\left(\tau_{f3} - \tau\right)^{m_{33}}}{\left(\tau_{f3} - \tau_{f2}\right)^{m_{33}}} + F_{33}\frac{\left(\tau_{f3} - \tau\right)^{n_{33}}}{\left(\tau_{f3} - \tau_{f2}\right)^{n_{33}}}\tau_{f2}\mathcal{D}_{\tau}^{\lambda_{33}}\sigma_{31} \tag{80}$$

where a_3, p_3, n_{32}, n_{33}, F_{32}, F_{33}, m_{32} and m_{33} are constant gain coefficients, $a_3 > 0$, $p_3 > 0$, $n_{32} > 1$, $n_{33} > 1$, $m_{32} > 1$, $m_{33} > 1$, $m_{32} - n_{32} + 1 \neq 0$, $m_{33} - n_{33} + 1 \neq 0$, $\lambda_{32} \in \boldsymbol{R}$, $\lambda_{32} \neq 0$, $\lambda_{33} \in \boldsymbol{R}$, $\lambda_{33} \neq 0$, $C_{31} = -e_{31}\left(\tau_{f2}\right)e^{a_3}$, $C_{32} = -\zeta_{32}(\tau_{f2}) - \frac{n_{32}\zeta_{31}(\tau_{f2})}{(\tau_{f3}-\tau_{f2})}$ and $C_{33} = -\sigma_{32}(\tau_{f2}) - \frac{n_{33}\sigma_{31}(\tau_{f2})}{(\tau_{f3}-\tau_{f2})}$.

For simplicity, the three intermediate control quantities P_v, P_χ and P_γ are set to

$$\begin{cases} P_v = P\cos\varphi \\ P_\gamma = P\sin\varphi\cos\psi \\ P_\chi = P\sin\varphi\sin\psi \end{cases} \tag{81}$$

For Equation (75), the method presented in Theorem 1 is adopted; while for the two second-order nonlinear systems given in Equations (76) and (77), the method presented in Theorem 2 is employed. One can obtain

$$\begin{aligned} P_v = &-mg\sin\theta + mv\sin\theta\left(\frac{C_{31}p_3\left(\tau_{f3} - \tau\right)^{p_3-1}}{\left(\tau_{f3} - \tau_{f2}\right)^{p_3}e^{a_3\left(\tau_{f3}-\tau\right)^{p_3}/\left(\tau_{f3}-\tau_{f2}\right)^{p_3}}} + \right. \\ &\left.\frac{a_3p_3e_{31}\left(\tau_{f3} - \tau\right)^{p_3-1}}{\left(\tau_{f3} - \tau_{f2}\right)^{p_3}} - K_{31}\mathrm{sgn}(S_{31})\right) \end{aligned} \tag{82}$$

$$\begin{aligned} P_\gamma = &-mv^2\sin^3\gamma\left(\cos\chi\left(\frac{n_{32}\zeta_{32}}{\tau_{f3} - \tau} + \frac{n_{32}\zeta_{31}}{\left(\tau_{f3} - \tau\right)^2} - C_{32}m_{32}\frac{\left(\tau_{f3} - \tau\right)^{m_{32}-1}}{\left(\tau_{f3} - \tau_{f2}\right)^{m_{32}}} + \right.\right. \\ &K_{32}\mathrm{sgn}(S_{32}) - n_{32}F_{32}\frac{\left(\tau_{f3} - \tau\right)^{n_{32}-1}}{\left(\tau_{f3} - \tau_{f2}\right)^{n_{32}}}\tau_{f2}\mathcal{D}_{\tau}^{\lambda_{32}}\zeta_{31} + \\ &F_{32}\frac{\left(\tau_{f3} - \tau\right)^{n_{32}}}{\left(\tau_{f3} - \tau_{f2}\right)^{n_{32}}}\tau_{f2}\mathcal{D}_{\tau}^{\lambda_{32}+1}\zeta_{31}\Bigg) + \sin\chi\left(\frac{n_{33}\sigma_{32}}{\tau_{f3} - \tau} + \frac{n_{33}\sigma_{31}}{\left(\tau_{f3} - \tau\right)^2} - \right. \\ &C_{33}m_{33}\frac{\left(\tau_{f3} - \tau\right)^{m_{33}-1}}{\left(\tau_{f3} - \tau_{f2}\right)^{m_{33}}} + K_{33}\mathrm{sgn}(S_{33}) - n_{33}F_{33}\frac{\left(\tau_{f3} - \tau\right)^{n_{33}-1}}{\left(\tau_{f3} - \tau_{f2}\right)^{n_{33}}}\tau_{f2}\mathcal{D}_{\tau}^{\lambda_{33}}\sigma_{31} + \\ &\left.\left.F_{33}\frac{\left(\tau_{f3} - \tau\right)^{n_{33}}}{\left(\tau_{f3} - \tau_{f2}\right)^{n_{33}}}\tau_{f2}\mathcal{D}_{\tau}^{\lambda_{33}+1}\sigma_{31}\right)\right) - mg\cos\gamma \end{aligned} \tag{83}$$

$$
\begin{aligned}
P_\chi = & mv^2\sin^2\gamma\left(\sin\chi\left(\frac{n_{32}\zeta_{32}}{\tau_{f3}-\tau}+\frac{n_{32}\zeta_{31}}{\left(\tau_{f3}-\tau\right)^2}-C_{32}m_{32}\frac{\left(\tau_{f3}-\tau\right)^{m_{32}-1}}{\left(\tau_{f3}-\tau_{f2}\right)^{m_{32}}}+\right.\right. \\
& K_{32}\mathrm{sgn}(S_{32})-n_{32}F_{32}\frac{\left(\tau_{f3}-\tau\right)^{n_{32}-1}}{\left(\tau_{f3}-\tau_{f2}\right)^{n_{32}}}\tau_{f2}\mathcal{D}_\tau^{\lambda_{32}}\zeta_{31} \\
& \left.+F_{32}\frac{\left(\tau_{f3}-\tau\right)^{n_{32}}}{\left(\tau_{f3}-\tau_{f2}\right)^{n_{32}}}\tau_{f2}\mathcal{D}_\tau^{\lambda_{32}+1}\zeta_{31}\right)-\cos\chi\left(\frac{n_{33}\sigma_{32}}{\tau_{f3}-\tau}+\frac{n_{33}\sigma_{31}}{\left(\tau_{f3}-\tau\right)^2}\right. \\
& -C_{33}m_{33}\frac{\left(\tau_{f3}-\tau\right)^{m_{33}-1}}{\left(\tau_{f3}-\tau_{f2}\right)^{m_{33}}}+K_{33}\mathrm{sgn}(S_{33})- \\
& \left.\left.n_{33}F_{33}\frac{\left(\tau_{f3}-\tau\right)^{n_{33}-1}}{\left(\tau_{f3}-\tau_{f2}\right)^{n_{33}}}\tau_{f2}\mathcal{D}_\tau^{\lambda_{33}}\sigma_{31}+F_{33}\frac{\left(\tau_{f3}-\tau\right)^{n_{33}}}{\left(\tau_{f3}-\tau_{f2}\right)^{n_{33}}}\tau_{f2}\mathcal{D}_\tau^{\lambda_{33}+1}\sigma_{31}\right)\right)
\end{aligned}
\tag{84}
$$

where K_{31}, K_{32} and K_{33} are constants, $K_{31} > d_{31}$, $K_{32} > d_{32}$ and$K_{33} > d_{33}$.

To sum up, the control quantities can be obtained

$$
\begin{cases}
\psi = \arctan(P_\chi / P_\gamma) \\
\varphi = \arctan(P_\gamma / (P_v \cos\psi)) \\
P = P_v / \cos\varphi
\end{cases}
\tag{85}
$$

The flowchart of the multi-phase integrated guidance system proposed in this paper is shown in Figure 3.

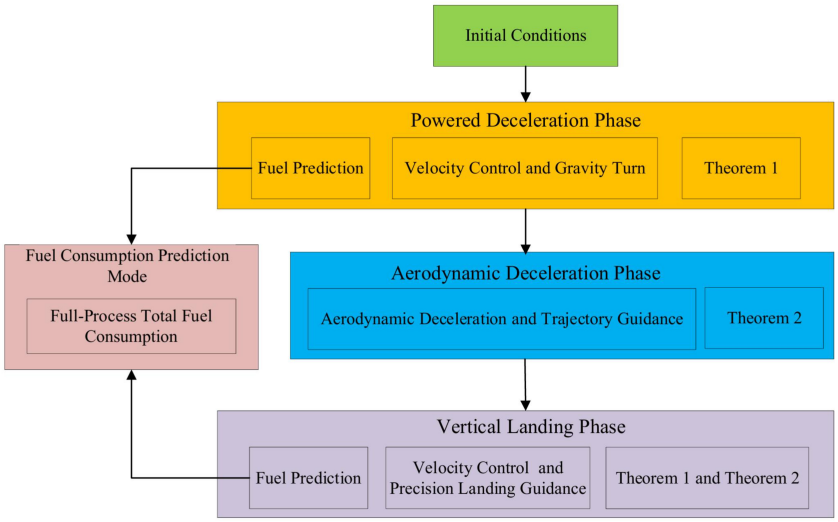


Figure 3. The flowchart of the multi-phase integrated guidance system.

4. Fuel Consumption Prediction Model

Based on the sliding mode guidance method mentioned above, this section proposes a new fuel consumption estimation method during the rocket recovery process to solve the problem of residual fuel constraints. Assume that the unloaded mass of the rocket without fuel is m_{f3}. The analytical formula of mass variation with pseudo height variable τ is calculated theoretically, and the initial mass m_{f2} of the rocket in the vertical landing stage is obtained. Let m_{f1} denote the rocket mass when the powered-deceleration phase finishes, and the initial mass m_0 can be calculated by adopting the same calculation method. Since

the mass of the aerodynamic deceleration section remains unchanged, there is $m_{f1} = m_{f2}$. Ultimately, the rocket's initial mass m_0 is derived according to its unloaded mass m_{f3}, so as to obtain the theoretical fuel consumption $\Delta m = m_0 - m_{f3}$.

The engine deflection angles φ and ψ are small in the vertical landing stage. Assuming $\varphi = 0$ and $\psi = 0$, Equation (82) can be simplified to

$$\begin{aligned} P = &- mg\sin\gamma + mv\sin\gamma\Big(a_3 p_3 e_{31}\left(\tau_{f3}-\tau\right)^{p_3-1}/\left(\tau_{f3}-\tau_{f2}\right)^{p_3} - K_{31}\mathrm{sgn}(S_{31}) + \\ &C_{31}p_3\left(\tau_{f3}-\tau\right)^{p_3-1}/\left(\left(\tau_{f3}-\tau_{f2}\right)^{p_3} e_{31} e^{a_3\left(\tau_{f3}-\tau\right)^{p_3}/\left(\tau_{f3}-\tau_{f2}\right)^{p_3}}\right)\Big) \end{aligned} \tag{86}$$

Bring Equation (86) into Equation (50), it yields

$$m' + \frac{m}{I_{sg}}\left(\frac{g}{v} - \left(\begin{array}{c} \frac{a_3 p_3 e_{31}\left(\tau_{f3}-\tau\right)^{p_3-1}}{\left(\tau_{f3}-\tau_{f2}\right)^{p_3}} - K_{31}\mathrm{sgn}(S_{31}) + \\ \frac{C_{31}p_3\left(\tau_{f3}-\tau\right)^{p_3-1}}{\left(\tau_{f3}-\tau_{f2}\right)^{p_3} e^{a_3\left(\tau_{f3}-\tau\right)^{p_3}/\left(\tau_{f3}-\tau_{f2}\right)^{p_3}}} \end{array}\right)\right) = 0 \tag{87}$$

According to Equation (10), the analytical formula of velocity error e_{31} in vertical landing phase can be obtained

$$e_{31} = -C_{31}\left(\tau_{f3}-\tau\right)^{p_3}/\left(\left(\tau_{f3}-\tau_{f2}\right)^{p_3} e^{a_3\left(\tau_{f3}-\tau\right)^{p_3}/\left(\tau_{f3}-\tau_{f2}\right)^{p_3}}\right) \tag{88}$$

From Equation (70), one can get $v = e_{31} + v_{f3}$, and bring it and Equation (88) into Equation (87) to obtain Equation (89).

$$m' + m\left(\begin{array}{c} \frac{g\left(\tau_{f3}-\tau_{f2}\right)^{p_3} e^{a_3\left(\tau_{f3}-\tau\right)^{p_3}/\left(\tau_{f3}-\tau_{f2}\right)^{p_3}}}{I_{sg} v_{f3}\left(\tau_{f3}-\tau_{f2}\right)^{p_3} e^{a_3\left(\tau_{f3}-\tau\right)^{p_3}/\left(\tau_{f3}-\tau_{f2}\right)^{p_3}} - C_{31}\left(\tau_{f3}-\tau\right)^{p_3}} + \\ \frac{K_{31}\mathrm{sgn}(S_{31})}{I_{sg}} + \frac{a_3 p_3 C_{31}\left(\tau_{f3}-\tau\right)^{2p_3-1}}{I_{sg}\left(\tau_{f3}-\tau_{f2}\right)^{2p_3} e^{a_3\left(\tau_{f3}-\tau\right)^{p_3}/\left(\tau_{f3}-\tau_{f2}\right)^{p_3}}} - \\ \frac{C_{31}p_3\left(\tau_{f3}-\tau\right)^{p_3-1}}{I_{sg}\left(\tau_{f3}-\tau_{f2}\right)^{p_3} e^{a_3\left(\tau_{f3}-\tau\right)^{p_3}/\left(\tau_{f3}-\tau_{f2}\right)^{p_3}}} \end{array}\right) = 0 \tag{89}$$

For convenience, four intermediate variables are set.

$$D_{31} = \frac{g}{I_{sg}}\int_{\tau_{f2}}^{\tau_{f3}} \frac{\left(\tau_{f3}-\tau_{f2}\right)^{p_3} e^{a_3\left(\tau_{f3}-\tau\right)^{p_3}/\left(\tau_{f3}-\tau_{f2}\right)^{p_3}}}{v_{f3}\left(\tau_{f3}-\tau_{f2}\right)^{p_3} e^{a_3\left(\tau_{f3}-\tau\right)^{p_3}/\left(\tau_{f3}-\tau_{f2}\right)^{p_3}} - C_{31}\left(\tau_{f3}-\tau\right)^{p_3}} d\tau \tag{90}$$

$$D_{32} = \frac{K_{31}\left(\tau_{f3}-\tau_{f2}\right)}{I_{sg}} \geq \int_{\tau_{f2}}^{\tau_{f3}} K_{31}\mathrm{sgn}(S_{31})d\tau \tag{91}$$

$$\begin{aligned} D_{33} &= \int_{\tau_{f2}}^{\tau_{f3}} -\frac{C_{31}p_3\left(\tau_{f3}-\tau\right)^{p_3-1}}{I_{sg}\left(\tau_{f3}-\tau_{f2}\right)^{p_3} e^{a_3\left(\tau_{f3}-\tau\right)^{p_3}/\left(\tau_{f3}-\tau_{f2}\right)^{p_3}}} d\tau \\ &= \frac{-C_{31}p_3}{I_{sg}\left(\tau_{f3}-\tau_{f2}\right)^{p_3}}\int_{\tau_{f2}}^{\tau_{f3}} \left(\tau_{f3}-\tau\right)^{p_3-1} e^{-a_3\left(\tau_{f3}-\tau\right)^{p_3}/\left(\tau_{f3}-\tau_{f2}\right)^{p_3}} d\tau \\ &= \frac{-C_{31}p_3}{I_{sg}\left(\tau_{f3}-\tau_{f2}\right)^{p_3}} \frac{\left(\tau_{f3}-\tau_{f2}\right)^{p_3}}{a_3 p_3}\left(1-e^{-a_3}\right) = \frac{-C_{31}}{I_{sg}a_3}\left(1-e^{-a_3}\right) \end{aligned} \tag{92}$$

$$
\begin{aligned}
D_{34} &= \int_{\tau_{f2}}^{\tau_{f3}} \frac{a_3 p_3 C_{31}\left(\tau_{f3}-\tau\right)^{2p_3-1}}{I_{sg}\left(\tau_{f3}-\tau_{f2}\right)^{2p_3} e^{a_3\left(\tau_{f3}-\tau\right)^{p_3}/\left(\tau_{f3}-\tau_{f2}\right)^{p_3}}} d\tau \\
&= \frac{a_3 p_3 C_{31}}{I_{sg}\left(\tau_{f3}-\tau_{f2}\right)^{2p_3}} \int_{\tau_{f2}}^{\tau_{f3}} \frac{\left(\tau_{f3}-\tau_{f2}\right)^{p_3}}{a_3 p_3} \left(\tau_{f3}-\tau\right)^{p_3} de^{-a_3\left(\tau_{f3}-\tau\right)^{p_3}/\left(\tau_{f3}-\tau_{f2}\right)^{p_3}} \\
&= \frac{C_{31}}{I_{sg}\left(\tau_{f3}-\tau_{f2}\right)^{p_3}} \left(\begin{array}{l} \left(\tau_{f3}-\tau_{f2}\right)^{p_3} e^{-a_3} + \\ p_3 \int_{\tau_{f2}}^{\tau_{f3}} \left(\tau_{f3}-\tau\right)^{p_3-1} e^{-a_3\left(\tau_{f3}-\tau\right)^{p_3}/\left(\tau_{f3}-\tau_{f2}\right)^{p_3}} d\tau \end{array} \right) \\
&= \frac{C_{31}}{I_{sg}\left(\tau_{f3}-\tau_{f2}\right)^{p_3}} \left(\left(\tau_{f3}-\tau_{f2}\right)^{p_3} e^{-a_3} + \frac{\left(\tau_{f3}-\tau_{f2}\right)^{p_3}\left(1-e^{-a_3}\right)}{a_3} \right) \\
&= \frac{C_{31}}{I_{sg} a_3}\left(1-e^{-a_3}-a_3 e^{-a_3}\right)
\end{aligned}
\tag{93}
$$

where D_{31} is defined as the potential energy factor, which is used to overcome the gravitational potential energy of the rocket. D_{32} is defined as the anti-disturbance factor, which is used to overcome uncertain disturbances. $D_{33}+D_{34}$ is defined as the kinetic energy factor, which is used to cancel out the rocket's kinetic energy. $C_{31} = -e_{31}\left(\tau_{f2}\right)e^{a_3} = \left(v_{f3}-v_{f2}\right)e^{a_3}$, and the sum of the kinetic energy factors is

$$
D_{33}+D_{34} = \frac{\left(v_{f2}-v_{f3}\right)}{I_{sg}} \tag{94}
$$

The relationship between initial mass m_{f2} and falling mass m_{f3} can be obtained by combining Equation (89) during the vertical landing stage.

$$
m_{f3} = m_{f2} e^{-(D_{31}+D_{32}+D_{33}+D_{34})} = m_{f2} e^{-\left(D_{31}+\frac{K_{31}\left(\tau_{f3}-\tau_{f2}\right)}{I_{sg}}+\frac{\left(v_{f2}-v_{f3}\right)}{I_{sg}}\right)} \tag{95}
$$

Similarly, the potential energy factor D_{11}, anti-disturbance factor D_{12}, kinetic energy factor $D_{13}+D_{14}$ in the powered deceleration phase can be obtained as

$$
\begin{aligned}
D_{11} &= \frac{g}{I_{sg}} \int_{\tau_0}^{\tau_{f1}} \frac{\left(\tau_{f1}-\tau_0\right)^{p_1} e^{a_1\left(\tau_{f1}-\tau\right)^{p_1}/\left(\tau_{f1}-\tau_0\right)^{p_1}}}{v_{f1}\left(\tau_{f1}-\tau_0\right)^{p_1} e^{a_1\left(\tau_{f1}-\tau\right)^{p_1}/\left(\tau_{f1}-\tau_0\right)^{p_1}} - C_1\left(\tau_{f1}-\tau\right)^{p_1}} d\tau \\
D_{12} &= \frac{K_1\left(\tau_{f1}-\tau_0\right)}{I_{sg}} \geq \int_{\tau_0}^{\tau_{f1}} K_1 \mathrm{sgn}(S_1) d\tau \\
D_{13}+D_{14} &= \frac{\left(v_0-v_{f1}\right)}{I_{sg}}
\end{aligned}
\tag{96}
$$

From Equation (96), one can get the relationship between m_0 and m_{f1}.

$$
m_{f1} = m_0 e^{-(D_{11}+D_{12}+D_{13}+D_{14})} = m_0 e^{-\left(D_{11}+\frac{K_1\left(\tau_{f1}-\tau_0\right)}{I_{sg}}+\frac{\left(v_0-v_{f1}\right)}{I_{sg}}\right)} \tag{97}
$$

The thrust of the engine in the aerodynamic deceleration section is zero; it allows $m_{f1} = m_{f2}$. If the unloaded mass of the rocket without fuel is m_{f3}, the theoretical value

of the initial mass of the rocket in the powered deceleration stage can be obtained from Equations (95) and (97).

$$m_0 = m_{f3} e^{\left(D_{11}+D_{31}+\frac{K_1\left(\tau_{f1}-\tau_0\right)}{I_{sg}}+\frac{K_{31}\left(\tau_{f3}-\tau_{f2}\right)}{I_{sg}}+\frac{\left(v_0-v_{f1}\right)}{I_{sg}}+\frac{\left(v_{f2}-v_{f3}\right)}{I_{sg}} \right)} \tag{98}$$

The theoretical fuel required for rocket recovery is $\Delta m = m_0 - m_{f3}$.
Key-used parameters in this paper are listed in Appendix A.

Remark 2. *Existing analytical guidance methods with speed constraints are usually difficult to predict the fuel consumption during the guidance process in advance, while the proposed prediction model can estimate the fuel consumption of the rocket during the braking process through two modes. The first mode is that if the initial mass of the rocket entering the powered deceleration phase or vertical landing phase is known, the fuel consumption during the rocket's braking and deceleration process can be calculated. The second mode is that if the unloaded mass of the rocket without fuel is known, the minimum remaining fuel required before the rocket's braking and deceleration can be estimated. It is worth noting that this method considers the influence of interference, which means the calculated result is the theoretical fuel consumption that is slightly higher than the actual fuel consumption. Combined with the guidance law of the aerodynamic reduction stage, a speed upper limit is set to estimate the initial speed of the vertical landing stage.*

Remark 3. *The correlations between key parameters and fuel consumption are summarized as follows. Fuel consumption declines by reducing p_3 or increasing a_3 when $(-1)^{p_3} > 0$. For $(-1)^{p_3} < 0$, fuel consumption reduction can be achieved by increasing p_3 or decreasing a_3. Nevertheless, such parameter adjustments generally require a broader impulse-adjustment range of the engine. Provided that the upper bound of velocity-related disturbance is denoted as $|d_{31}|_{max}$, the parameter-selection criterion for the anti-disturbance factor is defined as $K_{31} > |d_{31}|_{max} e^a$. The kinetic energy factor is governed by the initial and terminal velocities, and it can be tuned by adjusting the initial-stage velocity and landing-terminal velocity.*

5. Simulation and Analysis

Numerical simulations with four typical cases are conducted in this section to validate the proposed FOTSMG law. Firstly, multiple landing-site scenarios are simulated to validate the universality of the designed guidance law and fuel calculation strategy. Secondly, the influences of the rocket's unloaded mass, initial speed and initial altitude on fuel consumption are discussed. Then, the effects of different guidance parameters on the flight trajectory and fuel consumption are analyzed. Finally, Monte Carlo numerical simulation is performed to test the robustness of the developed method. Apart from specially specified conditions, all simulation cases share identical initial parameters summarized in Tables 1 and 2.

Table 1. Model initial parameters.

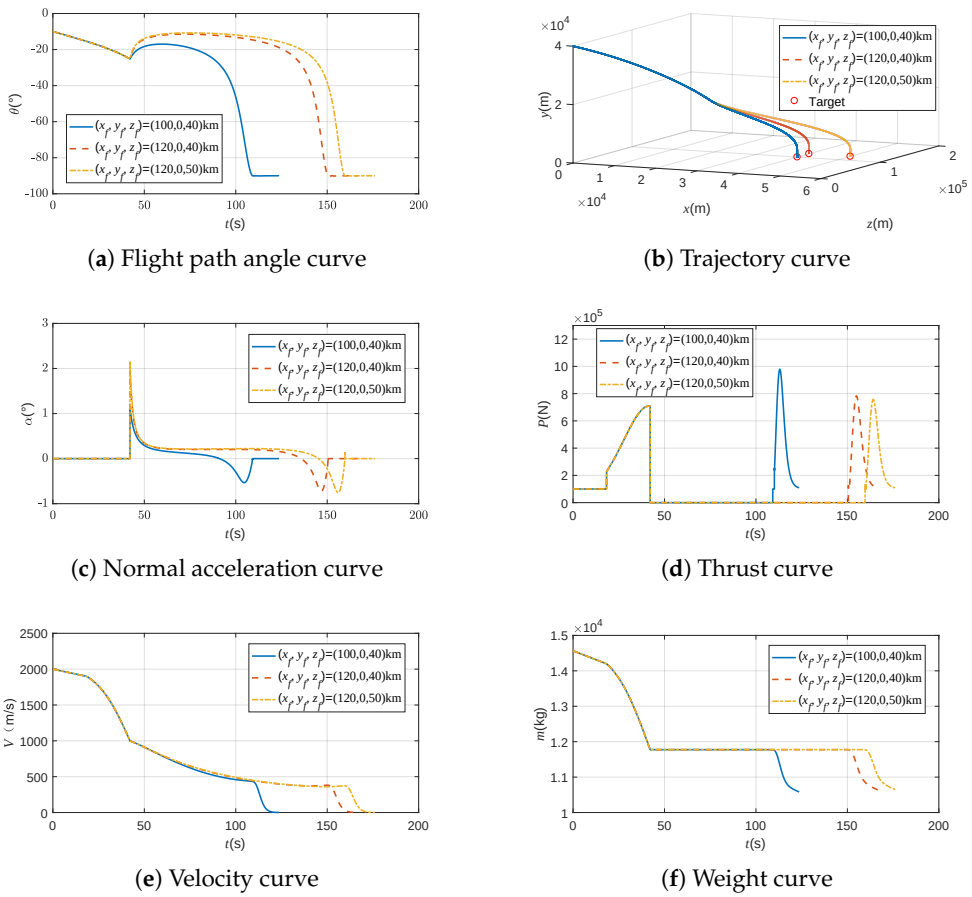
Parameters	Value	Parameters	Value
(x_0, y_0, z_0)	(0, 40, 0) km	y_{f1}	20 km
(x_f, y_{f3}, z_f)	(100, 0, 40) km	y_{f2}	2 km
v_0	2000 m/s	v_{f1}	1000 m/s
θ_0	−10 deg	v_{f2}	500 m/s
m_{f3}	10,000 kg	v_{f3}	1 m/s
g	9.8 m/s^2	I_{sg}	5000 m/s
$[P_{\min}, P_{\max}]$	[100, 1000] kN	$[a_{\min}, a_{\max}]$	[−100, 100] m/s

Table 2. Controller parameters.

Parameters	Value	Parameters	Value	Parameters	Value	Parameters	Value
a_1	1	F_{21}	-5×10^{-4}	p_3	1	F_{33}	1×10^{-6}
p_1	1	F_{22}	1×10^{-5}	K_{31}	5×10^{-2}	λ_{32}	-0.4
K_1	2×10^{-3}	λ_{21}	-0.4	n_{32}	3	λ_{33}	-0.4
n_{21}	3	λ_{22}	-0.4	n_{33}	3	K_{32}	1×10^{-4}
n_{22}	3	K_{21}	3×10^{-3}	m_{32}	2	K_{33}	1×10^{-4}
m_{21}	2	K_{22}	1×10^{-3}	m_{33}	2		
m_{22}	2	a_3	1	F_{32}	1×10^{-6}		

Case 1 Simulations with different landing sites

This case gives the simulation cases of three landing points, (100, 0, 40) km, (100, 0, 50) km and (120, 0, 50) km respectively. From Equation (98) and the rocket's no-load weight, the theoretical fuel consumption for the RLV recovery process is 4565kg, which means m_0 = 14,565 kg .The corresponding simulation outcomes are illustrated in Figure 4 and Table 3.



(**a**) Flight path angle curve (**b**) Trajectory curve

(**c**) Normal acceleration curve (**d**) Thrust curve

(**e**) Velocity curve (**f**) Weight curve

Figure 4. Simulation results with different landing points.

Looking at Figure 4c–f, the rocket's push, normal acceleration, speed and available fuel meet the constraint requirements in all three simulations. Figure 4a,b are the angle and trajectory change curves of the rocket, which reveal that the RLV realizes vertical landing at the desired landing sites after passing through the powered deceleration and aerodynamic deceleration and vertical landing phase. As seen from Table 3, the speed error, position error and angle error of RLV during landing are small, which means that RLV can accurately realize vertical soft landing at three landing points. As depicted in Figure 4f, the total mass

of the launch vehicle stays nearly constant in the powered deceleration phase. Differences in fuel consumption mainly arise during the vertical-landing phase. Variations in landing-site positions lead to different flight durations of aerodynamic deceleration and divergent inlet velocities at the end-point of the aerodynamic deceleration phase, namely the starting point of the vertical-landing phase. Since the preset terminal landing velocity remains fixed, the required velocity reduction varies across cases and eventually produces discrepancies in fuel consumption. According to the data in Table 3, such fuel deviation occupies only a small proportion of the total fuel consumption over the whole booster-recovery flight. The weight of the rocket landing is slightly greater than that of the rocket unloaded, which indicates that the theoretical fuel consumption calculated by Equation (98) meets the actual requirements. The remaining fuel is reserved for anti-jamming purposes.

Table 3. Results with different landing sites.

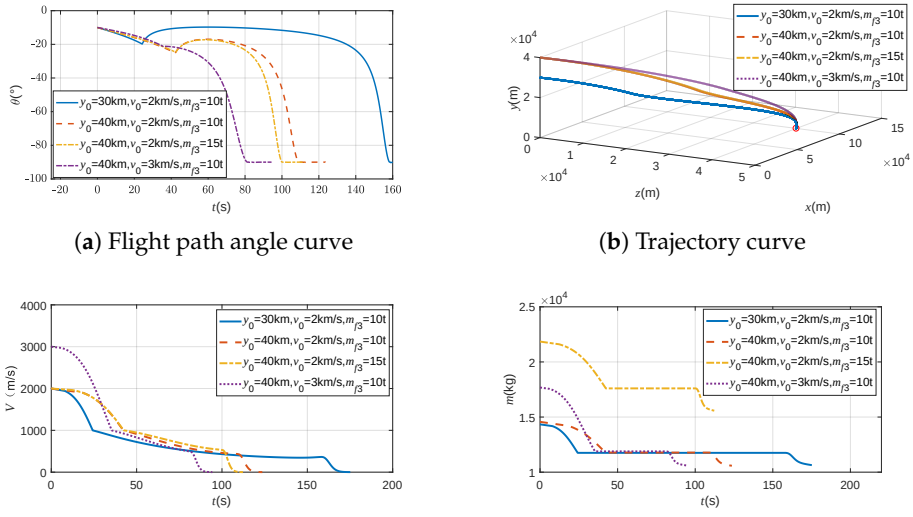
Landing Sites	(100, 0, 40) km	(100, 0, 50) km	(120, 0, 50) km
Landing distance errors (m)	5.69×10^{-10}	5.30×10^{-10}	3.92×10^{-10}
Landing angle errors (deg)	1.74×10^{-2}	1.06×10^{-2}	1.32×10^{-2}
Landing speeds errors (m/s)	1.10×10^{-1}	8.67×10^{-2}	8.35×10^{-2}
Rocket weight at landing (kg)	10,581	10,640	10,648
v_{f1} (m/s)	999.65	999.65	999.65

Case 2 Simulations with different rocket's no-load weights, initial speeds and initial heights

To validate the adaptability of the designed guidance scheme and the reliability of the fuel-estimation strategy under different no-load weights, initial speeds and initial heights of the rocket, four simulations are carried out in this case. Relevant initial-state parameters are listed in Tables 1, 2 and 4, and Figure 5 presents the corresponding simulation outcomes.

Table 4. Results with different initial conditions.

Simulation Order	Initial Height (km)	Initial Speed (m/s^2)	No-Load Weight (kg)	Theoretical Fuel Consumption (kg)
First	30	2	10,000	4337
Second	40	2	10,000	4565
Third	40	2	15,000	6848
Fourth	40	3	10,000	7679



(**a**) Flight path angle curve

(**b**) Trajectory curve

(**c**) Velocity curve

(**d**) Weight curve

Figure 5. Simulation results with different initial conditions.

For all simulations, the average landing position error is 2.63×10^{-9} m, the average landing angle error is 1.16×10^{-2} deg, and the average deviation for landing velocity is 0.121 m/s, which shows that the guidance law has high control accuracy and good applicability. Seen from Figure 5d that the theoretical fuel consumption meets the actual demand, which shows that the fuel calculation method is correct. From Figure 5b,c, the no-load weight of the rocket has little effect on the recovery trajectory, and the recovery time of heavier rockets is shorter. The greater the initial speed, the shorter the recovery time of the rocket and the greater the fuel consumption. Under a low-initial-altitude condition, the rocket spends a longer duration completing position adjustment within the aerodynamic deceleration phase, thereby leading to the maximum total recovery time.

Case 3 Simulations with different controller parameters

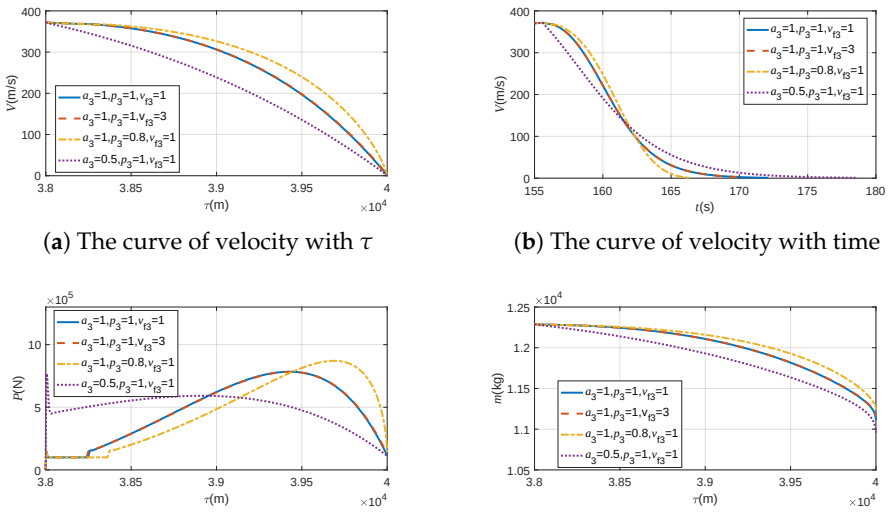
According to Equation (90), different controller parameters can affect the potential energy factor of fuel consumption. By analyzing how different parameters influence fuel-consumption performance within the vertical-landing stage, this case verifies that parameter tuning can regulate the total fuel expenditure during the RLV recovery process. Detailed simulation settings are summarized in Table 5, where the initial mass of the RLV is fixed at m_0 = 15,000 kg for all simulation groups. The corresponding numerical results are visualized in Table 6 and Figure 6.

Table 5. Results with different controller parameters.

The Simulation Order	a_3	p_3	v_{f3}
First	1	1	1 m/s
Second	1	1	3 m/s
Third	1	0.8	1 m/s
Fourth	0.5	1	1 m/s

Table 6. Landing weights of RLV with different simulations.

The Simulation Order	Landing Weights (kg)
First	11,113
Second	11,167
Third	11,243
Fourth	10,959



(**a**) The curve of velocity with τ (**b**) The curve of velocity with time

(**c**) The curve of thrust with τ (**d**) The curve of weight with τ

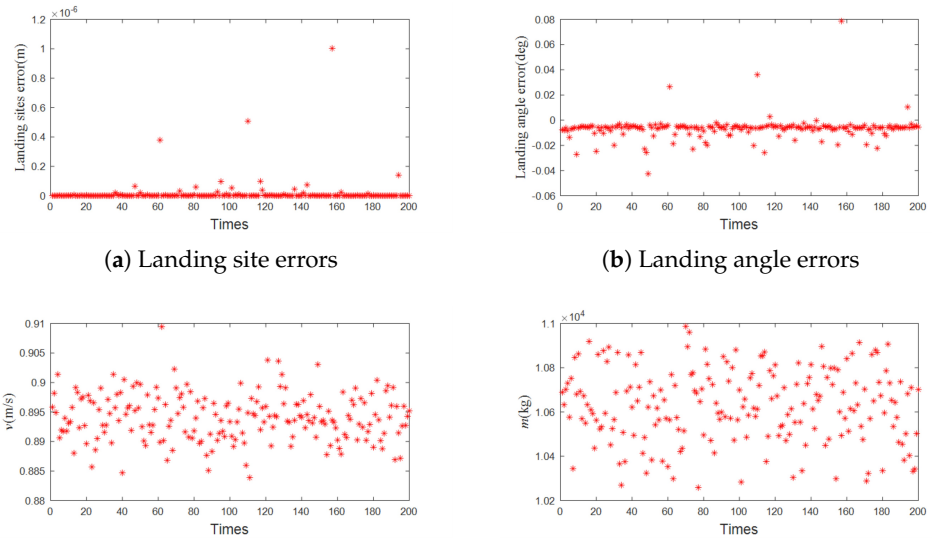
Figure 6. Simulation results with different controller parameters.

For all simulations, the average landing position error is 2.75×10^{-8} m, the average landing angle error is 1.45×10^{-2} deg, and the average landing speed error is 0.12 m/s^2, which shows that the change of parameters does not affect the guidance results. As shown in Figure 6a, with the given parameter declining, the rocket's velocity drops rapidly at the early stage and then decreases gently as altitude reduces, which lengthens the time consumed during the vertical-landing phase, as reflected in Figure 6b. The longer the rocket passes through the vertical landing phase means that it consumes more fuel (Seen from Table 6) and requires less thrust in the later stage (Seen from Figure 6c).

When p_3 decreases, the rocket's velocity drops mildly at first and then falls rapidly as the altitude reduces, shortening the flight duration of the vertical-landing phase. The shorter transit time of the rocket means that it consumes less fuel and requires more thrust in the later stage. When the expected landing speed increases in the current period, the speed curve is almost unchanged, and the time for the rocket to pass through the vertical landing phase is shorter, which means less fuel consumption. To sum up, the fuel consumption can be adjusted by changing the controller parameters.

Case 4 Monte Carlo simulations

Monte Carlo simulations are performed to comprehensively validate the robustness of the presented guidance strategy, where a total of 200 randomized trials are conducted in this case. In each simulation, random deviations of 2 %, 5 %, 10 %, 5 % and 5 % are generated for the initial weight, initial speed, lift and drag of the rocket and atmospheric density respectively. The outcomes of these Monte-Carlo tests are presented in Figure 7.



(**a**) Landing site errors (**b**) Landing angle errors

(**c**) Landing speed (**d**) Landing weight

Figure 7. Results with Monte Carlo simulations.

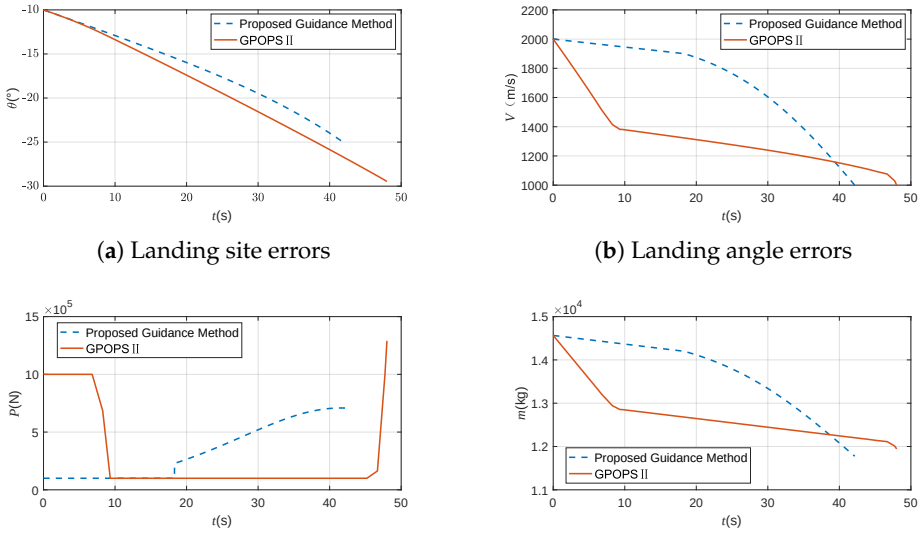
It can be observed from Figure 7a–c that the landing-position error is less than 1.2×10^{-6} m, the angular error is below 0.08 deg and the velocity error is limited to 0.12 m/s. The fuel consumption meets the landing-mission requirements in all simulation cases, which means the landing position, landing angle and landing speed of the rocket have high accuracy. Seen from Figure 7d, the landing weight of the rocket in all simulations is greater than the no-load weight of the rocket, which shows that the fuel consumption calculated in theory meets the actual demand. In conclusion, the designed FOTSMG law possesses favorable anti-disturbance performance.

Case 5 Comparative simulation

In this case, simulations are performed on the powered deceleration phase to compare fuel consumption during the braking process between the proposed method and GPOPS-II. The simulation outcomes are presented in Figure 8.

The fuel consumption of the proposed guidance method reaches 2789 kg, while the consumption obtained via GPOPS-II is 2621 kg, which reveals the fuel-consumption increment against GPOPS-II equals 6%. As illustrated in Figure 8, the lower fuel consumption of GPOPS-II stems from maximum thrust operation for rapid deceleration. Nevertheless, such a scheme lacks adaptability to unexpected emergencies during the deceleration phase. In addition, GPOPS-II only yields the fuel consumption for the theoretical trajectory. In the practical landing mission, the theoretical angle-of-attack and engine thrust profiles generated by GPOPS-II cannot guarantee precise landing.

Although the presented method fails to achieve fuel-optimal performance, its analytic expression enables online guidance computation. Compared with optimal-trajectory-tracking guidance, the proposed strategy delivers superior robustness and anti-disturbance capacity. Moreover, the fuel-prediction approach can evaluate the full-process fuel requirement in advance for booster recovery. Sufficient fuel reserve is guaranteed for terminal landing, and extra recovery cost caused by redundant residual fuel can be avoided.



(**a**) Landing site errors (**b**) Landing angle errors

(**c**) Landing speed (**d**) Landing weight

Figure 8. Results with comparative simulation.

6. Conclusions

Aiming at the vertical recovery problem of RLV, this paper proposes a full-phase guidance method combining FOTSMG and fuel prediction. The designed guidance law covers three phases: powered deceleration, aerodynamic deceleration, and vertical landing. Through the PTFOSMC structure, high-precision control of trajectory and speed is achieved, while the time-varying sliding mode surface ensures the global convergence of the system. By introducing potential energy, kinetic energy, and disturbance factors, the analytical fuel consumption model can effectively predict fuel demand during the mission planning phase, thus balancing the reliability and economy of the recovery mission. Simulation results show that landing-position error is less than 1.2×10^{-6} m, the angular error is below 0.08 deg and the velocity error is limited to 0.12 m/s, which indicates the proposed method can achieve accurate and stable vertical soft landing under various disturbance conditions, where both terminal position and speed errors meet the constraint requirements. Fuel consumption of the proposed method during the powered deceleration phase is merely

6% higher than the fuel-optimal result obtained from GPOPS-II, which implies the fuel prediction error is within a reasonable range. This study provides a systematic solution with both control performance and mission planning capability for the vertical recovery of RLV, and it has good theoretical value and application potential.

Several limitations remain in the present research. At present, the fuel-prediction model within the multi-phase integrated guidance framework only takes potential-energy, kinetic-energy and interference factors into account. Complex coupled parameters including engine thrust loss, time-varying atmospheric wind field and structural mass consumption are excluded. Furthermore, all simulation tests are completed based on an ideal vehicle dynamic model, while hardware-in-the-loop verification and real-flight experiments are not implemented. Restricted by the online-solving mechanism of analytical guidance, the trajectory generated by this method cannot reach fuel-optimality. In addition, the proposed guidance strategy is designed for the powered-deceleration, aerodynamic-deceleration and vertical-landing phases of reusable boosters. Guidance parameters have not been optimized for harsh conditions such as high-temperature reentry and aerothermal coupling disturbances. Future work will concentrate on adaptive adjustment under multiple constraints to improve environmental adaptability under extreme interference.

Author Contributions: Conceptualization, J.G. and Y.F.; methodology, J.G.; software, Y.F.; validation, J.G., T.S. and J.Z.; formal analysis, J.Z.; investigation, J.Z.; resources, Y.F.; data curation, J.G.; writing—original draft preparation, J.G.; writing—review and editing, Y.F. and T.S.; visualization, J.G.; supervision, Y.F.; project administration, Y.F. and T.S. All authors have read and agreed to the published version of the manuscript.

Funding: This research received no external funding.

Institutional Review Board Statement: Not applicable.

Informed Consent Statement: Not applicable.

Data Availability Statement: The raw data supporting the conclusions of this article will be made available by the authors upon request.

Acknowledgments: The author is grateful to the Editors and Reviewers for their valuable comments.

Conflicts of Interest: The authors declare that they have no conflict of interest.

Appendix A

Definitions of key parameters are presented in Table A1.

Table A1. The list of symbols.

Symbol	Definition
y_0	initial altitude at the start of the powered deceleration phase
v_0	initial velocity at the start of the powered deceleration phase
y_{f1}	minimum altitude for the powered deceleration phase
v_{f1}	terminal velocity for the powered deceleration phase
y_{f2}	minimum altitude of the aerodynamic deceleration phase
v_{f2}	terminal velocity of the aerodynamic deceleration phase
y_{f3}	landing altitude
v_{f3}	landing speed
v	flight velocity
γ	flight path angle
χ	trajectory deflection angle
m	mass of rocket
g	gravitational acceleration
α	angle of attack
μ	roll angle
I_{sg}	engine specific impulse
D	aerodynamic resistance

Table A1. *Cont.*

Symbol	Definition
L	aerodynamic lift, respectively
$\boldsymbol{F}_e$	centrifugal inertia force
$\boldsymbol{F}_k$	Coriolis inertia force
$\boldsymbol{d}_w$	uncertain disturbances
$\boldsymbol{P}_T$	the engine thrust
$\boldsymbol{\omega}_e$	Earth's rotation speed vector
φ	engine longitudinal gimbal angle
ψ	engine lateral gimbal angle
τ	$y_0 - y$
e_1	$v - v_f$
S_1	sliding mode function of powered deceleration phase
a_1, p_1, C_1	gain parameters for S_1
K_1	switching-term of powered deceleration phase
τ_{f2}	$y_{f1} - y_{f2}$
γ_f	desired flight-path angle
χ_f	desired terminal azimuth angle
S_{21}, S_{22}	sliding mode function of aerodynamic deceleration phase
n_{21}, F_{21}, m_{21}, n_{21}, λ_{21}, C_{21}	gain parameters for S_{21}
n_{22}, F_{22}, m_{22}, n_{22}, λ_{22}, C_{22}	gain parameters for S_{22}
K_{21}, K_{22}	switching-term of aerodynamic deceleration phase
S_{31}, S_{32}, S_{33}	sliding mode function of Vertical landing phase
τ_{f3}	$y_{f2} - y_{f3}$
a_3, p_3, C_{31}	gain parameters for S_{31}
n_{32}, F_{32}, m_{32}, n_{32}, λ_{32}, C_{32}	gain parameters for S_{32}
n_{33}, F_{33}, m_{33}, n_{33}, λ_{33}, C_{33}	gain parameters for S_{33}
K_{31}, K_{32}, K_{33}	switching-term of Vertical landing phase

References

1. Ren, H.; Ma, Y.J.; Jiang, B. Optimal fault-tolerant control of reusable launch vehicle with actuator faults using zero-sum differential game theory. *Aerosp. Sci. Technol.* **2025**, *160*, 110080. [CrossRef]
2. Gregorio, A.; Borgna, F.; Fusaro, R.; Narducci, G.; Viola, N. Eco-design vision for reusable vertical launch vehicles supported by multi-disciplinary design methodology and framework. *Aerosp. Sci. Technol.* **2026**, *174*, 111871. [CrossRef]
3. Onel, A.-I. Preliminary Definition of a Family of Partially Reusable Microlaunchers with the Aid of an MDO Approach. *Aerospace* **2026**, *13*, 159. [CrossRef]
4. Zhong, Y.; Liu, D.H.; Wang, C. Research Progress of Key Technologies for Typical Reusable Launcher Vehicles. *IOP Conf. Ser. Mater. Sci. Eng.* **2018**, *449*, 012008. [CrossRef]
5. Zhao, J.; He, X.Y.; Li, H.Y.; Lu, L. An adaptive optimization algorithm based on clustering analysis for return multi-flight-phase of VTVL reusable launch vehicle. *Acta Astronaut.* **2021**, *183*, 112–125. [CrossRef]
6. Li, Y.; Wei, C.Z.; He, Y.F.; Hu, R.Y. A convex approach to trajectory optimization for boost back of vertical take-off/vertical landing reusable launch vehicles. *J. Frankl. Inst.* **2021**, *358*, 3403–3423. [CrossRef]
7. Lee, G.J.; Jo, M.S.; Choi, J.Y. Comparison of Second-Stage Recovery Methods for Reusable Launch Vehicles Across Vehicle Scales. *Aerospace* **2026**, *13*, 79. [CrossRef]
8. Cheng, G.H.; Jing, W.X.; Gao, C.S. Recovery trajectory planning for the reusable launch vehicle. *Aerosp. Sci. Technol.* **2021**, *117*, 106965. [CrossRef]
9. Zhao, J.; Li, H.Y.; He, X.Y.; Huang, Y.C.; Liu, J.H.; Schiavo, A.L. Uncertainty Analysis for Return Trajectory of Vertical Takeoff and Vertical Landing Reusable Launch Vehicle. *Math. Probl. Eng.* **2020**, *2020*, 4313758. [CrossRef]
10. Su, Y.; Dai, Y.; Liu, Y. A hybrid hyper-heuristic whale optimization algorithm for reusable launch vehicle reentry trajectory optimization. *Aerosp. Sci. Technol.* **2021**, *119*, 107200. [CrossRef]
11. Liu, Z.; Cui, N.; Du, L.; Pu, J. Sequential Convex Programming for Reentry Trajectory Optimization Utilizing Modified hp-Adaptive Mesh Refinement and Variable Quadratic Penalty. *Aerospace* **2024**, *11*, 785. [CrossRef]
12. Yang, R.; Liu, X.; Song, Z. Rocket Landing Guidance Based on Linearization-Free Convexification. *J. Guid. Control Dyn.* **2024**, *47*, 217–232. [CrossRef]
13. Su, Y.; Liu, Y. Reentry trajectory optimization for reusable launch vehicle using marine predator whale optimizer and smoothing technique. *Aerosp. Sci. Technol.* **2025**, *158*, 109839. . [CrossRef]
14. Guadagnini, J.; De Zaiacomo, G.; Lavagna, M. Mission Performance Assessment of the Recovery and Vertical Landing of a Reusable Launch Vehicle. *Aerospace* **2024**, *11*, 35. [CrossRef]
15. Calkins, G.E.; Putnam, Z.R.; Woffinden, D. Multi-Objective Robust Trajectory Design for Powered Descent and Landing. In Proceedings of the AIAA SCITECH 2024 Forum, Orlando, FL, USA, 8–12 January 2024; pp. 2024–0327. [CrossRef]

16. Robbiani, T.; Sagliano, M.; Topputo, F.; Seywald, H. Fast Desensitized Optimal Control for Rocket-Powered Descent and Landing. *J. Guid. Control Dyn.* **2025**, *48*, 2480–2494. [CrossRef]
17. Li, W.; Ji, Y.; Sun, G. Reusable Launch Vehicle Landing Online Guidance and Control Based on ESO-MPC and Convex Optimization. *IEEE Access* **2026**, *14*, 30860–30871. [CrossRef]
18. Li, S.; Peng, Y. Command generator tracker based direct model reference adaptive tracking guidance for Mars atmospheric entry. *Adv. Space Res.* **2012**, *49*, 49–63. [CrossRef]
19. Cheng, L.; Wang, Z.B.; Gong, S.P. Adaptive control of hypersonic vehicles with unknown dynamics based on dual network architecture. *Acta Astronaut.* **2022**, *193*, 197–208. [CrossRef]
20. Tahk, M.J.; Moon, G.H.; Shim, S.W. Augmented Polynomial Guidance with Terminal Speed Constraints for Unpowered Aerial Vehicles. *Int. J. Aeronaut. Space Sci.* **2019**, *20*, 183–194. [CrossRef]
21. Danchick, R. Connecting gravity turn guidance dynamics to near planar missile motion geometry. *IET Radar Sonar Navig.* **2016**, *10*, 278–284. [CrossRef]
22. Zhao, Y.; Sheng, Y.Z.; Liu, X.D. Analytical impact time and angle guidance via time-varying sliding mode technique. *ISA Trans.* **2016**, *62*, 164–176. [CrossRef] [PubMed]
23. Zhou, H.Y.; Wang, X.G.; Cui, N.G. Glide guidance for reusable launch vehicles using analytical dynamics. *Aerosp. Sci. Technol.* **2020**, *98*, 105678. [CrossRef]
24. Huang, Y.C.; Li, H.Y.; Zhang, J.; Du, X. Mars Atmospheric Entry Guidance Design by Sliding Mode Disturbance Observer-Based Control. *Procedia Eng.* **2015**, *99*, 1062–1075. [CrossRef]
25. Ming, C.; Wang, X.M.; Sun, R.S. A novel non-singular terminal sliding mode control-based integrated missile guidance and control with impact angle constraint. *Aerosp. Sci. Technol.* **2019**, *94*, 105368. [CrossRef]
26. Sheng, Y.Z.; Zhuo, Z.; Xia, L. Fractional-order sliding mode control based guidance law with impact angle constraint. *Nonlinear Dyn.* **2021**, *106*, 425–444. [CrossRef]
27. Sheng, Y.Z.; Gan, J.H.; Xia, L. Predefined-time fractional-order time-varying sliding mode control and its application in hypersonic vehicle guidance law. *Nonlinear Dyn.* **2023**, *111*, 14177–14198. [CrossRef]
28. Caputo, M. On the Caputo operator of fractional calculus and C-Laguerre functions. *Geophys. J. R. Astron. Soc.* **1967**, *13*, 529–539. [CrossRef]
29. Podlubny, I. *Fractional Differential Equations*; Academic Press: Cambridge, MA, USA, 1999.
30. Diethelm, K. The mean value theorems and a Nagumo-type uniqueness theorem for Caputo's fractional calculus. *Fract. Calc. Appl. Anal.* **2012**, *15*, 304–313. [CrossRef]
31. Fahad, H.M.; Fernandez, A. Operational calculus for Caputo fractional calculus with respect to functions and the associated fractional differential equations. *Appl. Math. Comput.* **2021**, *409*, 126400. [CrossRef]

Disclaimer/Publisher's Note: The statements, opinions and data contained in all publications are solely those of the individual author(s) and contributor(s) and not of MDPI and/or the editor(s). MDPI and/or the editor(s) disclaim responsibility for any injury to people or property resulting from any ideas, methods, instructions or products referred to in the content.